# AN ELECTRET DOSIMETER CHARGED BY RADIATION—INDUCED IONIZATIONS IN AIR

by

Lawrence N. Ryner

Medical Physics Unit

McGill University, Montreal

July, 1990

A Thesis Submitted to the

Faculty of Graduate Studies and Research
in Partial Fulfillment
of the Requirements for the Degree of

Master of Science in Medical Physics

o Lawrence N. Ryner, 1990

Aline

4

Ad Majorem Dei Gloriam

# ABSTRACT

An electret radiation dosimeter for long-term personnel monitoring is described. The design of this prototype (a modified parallel-plate ionization chamber) and the associated isothermal electret charging technique are presented. In the charging process, an external voltage causes ions created in air by the passage of radiation to move towards, and become trapped on, a dielectric (e.g., Mylar, Teflon) that covers the measuring electrode, forming an electret. Once the external voltage is removed, the field across the sensitive volume is produced by the electret charge, such that during subsequent irradiation, ions opposite in sign to those on the electret surface are attracted to the electret thus depleting the charge layer in an amount proportional to the exposure. Further irradiation releases the remaining charge on the electret which is measured with an electrometer. This technique allows the electret to be charged, used in the field, and discharged in situ, without dismantling the dosimeter as is required with other electret dosimeters relying on corona charging or other forming methods. Calibration, energy dependence, exposure range, and guard-ring effects of the dosimeter are discussed. This electret dosimeter may prove to be a viable alternative to film dosimeters and TLDs, and is inherently superior because the measuring medium is air.

# RÉSUMÉ

Un dosimètre personnel électrostatique à port prolongé est présenté. La réalisation d'un prototype (une chambre d'ionisation à électrodes parallèles modifiée) ainsi que la technique isothermale de chargement à employer y sont décrites. Lorsqu'on charge ce dosimètre, un voltage extérieur permet au diélectrique recouvrant l'électrode (électret) de capturer les charges ioniques créees dans la couche d'air du dosimètre par le passage de rayonnements ionisants. Lorsqu'on retire le voltage de chargement, le champ électrique utilisé par le volume sensible d'air est produit par la charge déposée sur l'électret; toute irradiation subséquente produira une diminution de la charge de l'électret car ce dernier attire les charges ioniques de signe opposé. La charge ainsi annulée est donc directement proportionelle à l'exposition. La charge restante est mesurée sous irradiation à l'aide d'un électromètre. Il est donc possible de charger, d'utiliser et de décharger le dosimètre sur place, sans le démonter, contrairement aux dosimètres électrostatiques dont la charge électrique de l'électret est produite par un effet de couronne ou toute autre technique. La technique de calibration, les effets de l'anneau de garde sur le dosimètre et l'étendue adéquate des expositions y sont démontrés. Ce dosimètre pourrait éventuellement remplacer les dosimètres utilisant un film ou un cristal thermoluminescent puisque le dosimètre proposé est intrinsèquement supérieur car il utilise un volume d'air pour la mesure.

# ORIGINAL CONTRIBUTION

The suitability of a new electret charging and read—out technique for use in electret dosimetry is examined. An electret dosimeter was constructed to take full advantage of this technique which allows the charging of the dosimeter, measurement of the initial charge state, use in the field, determination of the final charge state, and the clearing of any remaining signal without requiring the dismantling of the dosimeter, as is required with other electret dosimeters.

Various properties of the dosimeter are detailed. The exposure range is shown to be appropriate for personnel dosimetry. Capabilities of the electrometer read—out technique, with charge measurement accuracies of fractions of a picocoulomb, allow minimum detectable exposures in the low milliroentgen range. Parameters affecting the upper limit to the exposure range, extending to hundreds of roentgen for certain dosimeter configurations, are discussed as well as the energy dependence of the dosimeter with its relation to the electrode spacing.

Electrode edge-effects are shown to have a drastic response on the dosimeter's response for certain configurations. Although these effects have generally been neglected, due to the nature of the dosimeter's response to irradiation, and to limits on its physical size, it is shown that they cannot be disregarded. Nonlinearities previously ascribed to a loss of saturation conditions may be related to this phenomenon. An analytic method of minimizing errors due to these nonlinearities is presented.

# **ACKNOWLEDGEMENTS**

I thank Dr. B. Gino Fallone for the invaluable encouragement, support, and criticism offered to me throughout the past year. His insight into the scientific method and the patience with which he has shared it will remain with me for years to come.

I also thank my fellow colleague, Mr. Brennan MacDonald, for many hours of fruitful discussion, Mr. Lajos Palotay for his help in the construction of the many prototype electret dosimeters, Mr. Matthew Podgorsak for assistance in the determination of the dosimeter's energy dependence, and Messrs. Joe Larkin and Paul Lefebvre for help with the electrical aspects of the project.

I thank my wife Susan for her love and constant support.

This study would not have been possible without the financial support of The Whitaker Foundation. Their help is gratefully acknowledged.

# TABLE OF CONTENTS

																							Page
	Abstra	ct	•		•	•	•	•	•	•		•	•	•	•	•	•	•		•	•		2
	Résum	é .			•	•			•														iı
	Origin	al Cont	rib	utio	n														•			•	iii
	Ackno	wledger	ner	ıts		•			•	•	•		•		•		•	•					iv
	Table	of Cont	ent	ts		•	•		•	•		•		•			•	•				•	υ
	List of	Figure	S			•	•	•		•			•		•		•	٠		•		•	viii
	List of	Tables	i			•	•	•	•	•	•	•			•	•	•	•		•			xıı
Chapt	er 1	INTRO	DD	UC	OIT	N																	
	1.1	Genera	d I	ntro	duc	tio	n			•	•	•	•	•	•	•	•	•	•	•	•	•	1
	1.2	Thesis	Oı	gani	zat	ion	l			•	•	•	•	•	•	•	•	•	•	•	•		1
Chapt	er 2	PERS	ON	NEI	DO	OS	IM	ΕΊ	RY	(													
	2.1	Introd	uct	ion		•	•	•	•	•	•	•	•	•	•	•	•	•		•	•		3
	2.2	Differe	ent	Pers	onr	ıel	Do	sin	net	ers							•	•	•				3
	2.3	Electro	et I	Dosi	met	гу																	
		2.3 1		Ele	ctre	ts		•			•	•				•					•	•	4
		2.3.2		For	mat	ioi	n o	f E	lect	rei	ts				•	•	•	•			•	•	5
		2.3.3		Bas	ic N	<b>I</b> et	ho	dol	ogy	,		•						•			•	•	5
		2.3.4		Oth	er l	Ele	ctr	e <b>t</b>	Dos	sim	ete	ers						•				•	6
		2.3.5		The	Pr	ор	ose	d E	Elec	tre	et I	Oos	im	ete	r				•	•	•	•	7
	Refere	nces		• •	•	•	•	•		•	•	•			•	•	•	•	•	•	•		8
Chapt	er 3	MATI	ERI	ALS	S A I	ND	M	ΕΊ	TH(	OD	S												
	3 1	Const	T11.0	tion	of t	ha	Da	nei r	nat	<b>0</b> T													10

3.2	Electrical	l Conta	cts		•	•		•			•	•			•	•		12
3.3	Electrode	e Detail	s			•		•			•		•	•	•	•	•	12
3.4	Radiation	n Sourc	es				•	•				•					•	14
3.5	Measurer	nents		•				•			•		•				•	15
Refere	ences			• 1		•		•	•	•	•	•	•	•		•		16
Chapter 4	THE EL	ECTRI	ET DO	SIM	ETE	ER												
4.1	Introduc	tion	• •	•		•			•	•	•		•	•	•	•	•	17
4.2	Dosimeter Charging/Discharging by Radiation— Induced Air—Ionization																	
	4.2.1	Introd	luction	l	•	•	•	•	•	•	•	•	•	•	•	•	•	17
	4.2.2	Dosim	eter C	harg	ing			•	•	•	•	•	•	•	•	•	•	18
	4.2.3	Dosim	neter D	isch	ergii	ıg			•	•	•	•	•	•	•	•	•	23
	4.2.4	The C	Charge	/ Disc	har	ge (	Cur	ve				•	•	•	•		•	27
4.3	Calibrat	ion		•		•	•	•	•	•	•	•	•	•	•	•	•	30
4.4	Sensitivi	ty		•		•	•	•	•	•	•	•	•		•		•	33
4.5	Exposur	e Rang	е															
	4.5.1	Maxi	mum E	Expos	sure			•	•		•		•	•	•	•		39
	4.5.2	Minir	num E	xpos	ure				•	•			•		•	•	•	48
4.6	Natural	Surface	e Char	ge D	ec <b>ay</b>	Me	ech	ani	sm	S								
	4.6.1	Intro	duction	n.	•		•	•	•	•					•		•	49
	4.6.2	Radia	ation—]	Indu	ced (	Con	du	ctiv	vity	7								52
	4.6.3	Trap	–Modu	ılate	d Mo	obil	ity								•	•		54
	4.6.4	Modi	ficatio	n of	Forr	nali	ism	l			•	•				•	•	56
4.7	Prepara	tion of	Teflon	Elec	tret	s									•	•	•	58
4.8	Differen				ıge					•				•	•	•	•	60

Refere	nces .	• •	• •	•	•	•	•	•	•	•	•	•	•	•	•	•	•	63
Chapter 5	ELECTRO	DE E	DGE	EFI	FEC	TS												
5.1	Introduction	n					•	•										65
5.2	Variation of the Guard-Ring Width																	
	5.2.1	The Gu	ard-	-Ring	g St	udy				•							•	66
	5.2.2	Calibra	tion	with	No	nlin	eari	tie	S									70
5.3	Variation of	of the	Colle	ctor	Rac	dius												
	5.3.1	The Co	llect	or St	udy	7					•						•	76
	5.3.2	The Ide	eal D	osim	ete	r Co	nlie	gura	atic	n							•	79
5.4	Spatial Ch	arge D	ensi t	y In	forr	nati	on							•	•	•		79
Refere	nces .		•		•			•	•		•			•	•	•	•	89
Chapter 6	ENERGY	DEPE	ENDI	ENC	E													
6.1	Introduction	on	•		•		•	•	•	•				•	•	•	•	90
6.2	Low Energ	gies	•		•		•	•	•	•	•			•	•	•	•	90
6.3	Intermedia	ate En	ergie	S		•		٠		•	•	•		•	•	•	•	91
6.4	High Ener	gies			•			•	•	•	•	•	•	•			•	94
6.5	Overall E	nergy l	Depe	nden	ce				•	•	•	•		•		•	•	95
Refere	ences		•		•	•		•	•	•	•	•	•	٠	•	٠	•	97
Chapter 7	CONCLU	SION																
7.1	Summary		٠		•						•				•			98
7.2	Future W	ork	•		•		•	•	•			•	•		•		•	102
Bibliography			•		•	•						•	•	•	•	•		104

# LIST OF FIGURES

		Page
Figure 3.1	(a) Schematic diagram of the electret dosimeter; (b) expanded view of the electrical connection; (c) the panhandle design of the electrodes.	11
Figure 4.1	(a) Schematic showing the measured current in and out of saturation for both the charging and discharging of the dosimeter; (b) the electrode/polymer/air/electrode interface.	19
Figure 4.2	A charge/discharge curve plotting (a) current density versus time and (b) charge density versus time.	28
Figure 4.3	The calibration factor as a function of exposure rate at 90 kVp (effective energy: 26 keV).	32
Figure 4.4	A charge/discharge curve of current density versus time showing effect of a collector not fully covered with polymer.	34
Figure 4.5	Charge/discharge curve of current density versus time for the same dosimeter as Fig. 4.2 except for the increased air—gap.	36
Figure 4.6	Calibration factor $k$ as a function of the air—gap $a$ at 90 kVp showing proportion of $k$ due to photoemission from the polarizing electrode and to direct x—ray interactions with air.	37

		Page
Figure 4.7	Calibration factor $k$ as a function of the air-gap $a$ for a	40
	cobalt-60 radiation source.	
Figure 4.8	Charge/discharge curve of current density versus time for the	43
	same dosimeter as Fig. 4.2 except for the increase of the	
	initial charging voltage.	
Figure 4.9	Discharge curves of charge density removed versus exposure	45
riguie 4.5		40
	for (a) constant air-gap and various initial charging voltages	
	and (b) constant voltage and various air-gaps.	
Figure 4.10	Maximum exposure before loss of saturation conditions as a	46
	function of charging voltage from the data in Fig. 4.9(a).	
Figure 4.11	Current density as a function of time after the charging of a	55
	dosimeter illustrating the current measured due to the decay	
	of surface charge of the unirradiated electret and the decrease	
	in the rate at which this charge is decaying.	
Figure 4.12	(a) Discharge curve for a virgin 75 $\mu$ m Tesson electret	59
	showing anomalous "tail" at end of discharge; (b) current	
	versus time for the end of the discharge curve showing effect	
	of an increased charge-up voltage on the tail.	

1

voltage and (b) for a different air-gap and voltage.

		Page
Figure 5.6	(a) Slope of the initial flat portion of the current profile versus calibration factor for different air—gaps and collector radii; (b) collector radius versus calibration factor.	80
Figure 5.7	(a) Surface charge density across the collector as a function of time during the discharge process; (b) the same data plotted at 25 second intervals.	84
Figure 5.8	Two discharge curves of current density versus time for the same dosimeter charged with different air—gaps but discharged with the same air—gap.	87
Figure 6.1	(a) Relative response of the dosimeter to low energy x-rays for two different dosimeter electrode—backings; (b) relative response at intermediate energies for different air—gaps.	92
Figure 6.2	(a) Schematic plot showing effect of the atomic number of or surrounding the sensitive volume on a dosimeter's energy dependence; (b) the overall energy dependence for the electret dosimeter.	93
Figure 6.3	Typical energy dependence curves for a filtered film badge and a LiF TLD.	96

# LIST OF TABLES

		Page
Table 4.1	The charge removed and the standard deviation of each single	<b>5</b> 0
	measurement for a dosimeter, repeated 8 times with the mean	
	charge removed, the standard deviation of the 8 values from	
	the mean, and the average standard deviation of each single	
	measurement.	
Table 4.2	Exposure range for an electret dosimeter with a 110 $\mu m$	51
	Mylar electret and a 19 mm collector radius assuming a	
	minimum error in charge measurement of 0.01 nC and a	
	maximum charge—up voltage of 1000V.	
Table 5.1	The total charge removed per unit area collector for different	81
	dosimeter configurations - for different air-gaps a and	
	voltages $V_o$ at different collector radii $c$ — showing the	
	increased charge density for smaller collector radii.	

# CHAPTER 1

#### INTRODUCTION

## 1.1 GENERAL INTRODUCTION

The ideal personnel dosimeter has yet to be developed. The thermoluminescent dosimeter currently in popular use is indeed a step beyond the film dosimeter used in the past. However it is not the ideal personnel dosimeter. Electret dosimeters are gradually overcoming developmental problems and may prove to be the personnel dosimeter of choice in the future. This work details a new, simpler method of charging and reading out electret dosimeters. Also discussed are alternate explanations of some phenomena which were previously attributed to the loss of saturation conditions. Results suggest that these phenomena may instead be related to the spatially dependent depletion of the electret charge layer when irradiated.

# 1.2 THESIS ORGANIZATION

Chapter 2 briefly describes some of the currently available personnel dosimeters. The field of electret dosimetry is then introduced with a definition and description of an electret and methods by which they are formed. An introductory description of the proposed electret dosimeter follows, with a summary of its differences from others proposed in the past. A list of references is provided at the end of each chapter.

In Chapter 3, the construction of the electret dosimeter, the radiation sources used, and the experimental set—up are detailed.

Chapter 4 describes the operation of the electret dosimeter beginning with a full explanation, both descriptive and analytic, of the isothermal charging technique used to form the electret and the manner in which the dosimeter is discharged by

operation of the dosimeter. The charge/discharge curve is presented and the calibration procedure, with the associated calibration factor, outlined. The effect of various parameters on the sensitivity of the dosimeter is then discussed followed by a full analysis of the exposure range limits, both maximum and minimum. This leads to a discussion of possible problems with the charging technique associated with radiation—induced conductivity in the polymer and other problems encountered with virgin Teflon polymers. A discussion of the differences between voltage and charge read—out closes the chapter.

Chapter 5 deals with a problem often neglected but unavoidable with the electret dosimeter due to its small size — electrode edge effects. The purpose of the guard—ring is outlined and a study is presented which outlines the drastic effect of a decrease in size of the guard—ring on the response of the dosimeter to irradiation. An analytic method by which to minimize the errors associated with this effect is then presented. Upon deciding on the maximum overall size of the dosimeter, a study is then presented which determines the ideal dosimeter configuration that maximizes sensitivity while minimizing electrode edge effects. This leads to a method by which spatial charge density information can be derived resulting in a full explanation of the reasons for the various seemingly anomalous results observed.

Chapter 6 details the energy dependence of the dosimeter, and methods to minimize this dependence at low, intermediate and high energies.

Chapter 7 summarizes some of the important findings and provides suggestions for future work on the electret dosimeter.

## CHAPTER 2

#### PERSONNEL DOSIMETRY

## 2.1 INTRODUCTION

A personnel dosimeter is a special type of integrating dosimeter. There are many different kinds of personnel dosimeters, but all must have certain common features. A personnel dosimeter must be lightweight and of fairly small size so that it is easily worn on the body and does not interfere with everyday activities. It must be physically and electrically rugged to endure considerable shock and vibration while still performing reliably. Environmental effects on the dosimeter—including different levels of, and rates of change of, humidity, temperature, and pressure—must be minimal since the dosimeter is expected to operate reliably in a variety of environmental conditions.

# 2.2 DIFFERENT PERSONNEL DOSIMETERS

Thermoluminescent dosimeters<sup>2</sup> rely on the radiation—induced lifting of electrons and holes into traps and their subsequent release by the application of heat resulting in the emission of light with the amount of light being the measuring signal. Advantages of this type of dosimetry include a very wide useful dose range, reusability, and the capability of computer—automated read—out. Disadvantages include lack of uniformity among TLDs requiring individual calibration, fading of the signal, light sensitivity leading to either fading of signal or increase of signal, and reader instability.

Film badges<sup>3</sup>, or photographic dosimeters, rely on the change in optical density of the developed photographic film produced by irradiation. The disadvantages of this type of dosimetry are numerous including the requirement of careful control of the wet—chemical development process, a large energy dependence,

and the problem of solarization, where the optical density begins to decrease at large doses leading to ambiguity as to the determination of dose.

Chemical dosimeters<sup>4</sup> (e.g., Fricke dosimeters) rely on the determination of a quantitative chemical change in an irradiated medium, be it gaseous, liquid or solid. The minimum sensitivity of such dosimeters is too high for personnel dosimetry. There are also problems with storage stability and temperature dependence.

Condenser—type ionization chambers<sup>5</sup> are very similar in concept to electret dosimeters except conductors are used as the charge storage medium whereas polymers are used in electret dosimeters. This results in a self—discharge rate of a few percent per week<sup>6</sup>, making them unsuitable for long—term personnel monitoring. Another drawback is that condenser chambers are susceptible to errors due to physical mishandling—an undesirable feature for a personnel dosimeter.

#### 2.3 ELECTRET DOSIMETRY

#### 2.3.1 Electrets

All electret dosimeters rely on the use of an electret. An electret is a piece of dielectric material exhibiting a quasi-permanent electrical charge?. This charge could be a polarization due to an alignment of dipoles or actual charge carriers which are physically trapped in the material. "Quasi-permanent" indicates that the charge remains in the electret for long periods of time. The term "electret" was coined by Heaviside<sup>8</sup> in 1885 and was used in analogy with the magnet, indicating that the electret is the electrostatic equivalent of a magnet. Heaviside reserved the word "electret" solely for materials with a permanent dipole polarization thus keeping the analogy with the magnet strict. The term was eventually used for materials containing both dipolar and monopolar charges.

Thus the main property of an electret is its ability to retain electrical charge for extended periods of time and it is this property that is exploited in its use as a charge storage medium in the electret dosimeter, and in many other applications. With the proper choice of electret material and electret forming method, charge decay time constants of 200 years<sup>9</sup> have been recorded at room temperature.

# 2.3.2 Formation of Electrets

There are a variety of methods available to form electrets. Electrets exhibiting a space charge are generally formed 10 by deposition of charge carriers through discharge processes, particle beams, contact electrification or other methods. Alternatively, charge carriers can be generated in the material by light, radiation, or heat, with the separation of these charges facilitated by the application of an electric field across the electret material. Dipolar electrets are generally charged through the locking in of a dipole orientation by applying an electric field to a material at an elevated temperature followed by a decrease in the temperature with the field still applied.

The method by which a radioelectret is formed is different from the electret formation method to be discussed in Section 4.2.2 in that the charge carriers are generated in the polymer material itself with the separation of these charge carriers facilitated by an electric field applied across the thickness of the electret. The doses and electric fields required to form such radioelectrets are very large  $^{11}$  – 30 krad with  $^{60}$ Co gamma rays and polarizing fields of 35 kV cm $^{-1}$ .

# 2.3.3 Basic Methodology

The basic methodology involved in the use of all electret dosimeters is the same:

1. A charge,  $q_i$ , is deposited on the polymer surface. This is accomplished in the electret-forming process.

- 2. The dosimeter is then used in the field with  $q_i$  being depleted by an amount,  $q_x$ , due to exposure to radiation.
- 3. The remaining charge,  $q_f$ , on the polymer surface is then determined either directly or indirectly through voltage measurements.
- 4.  $q_x$  is then calculated  $(q_x = q_1 q_f)$  and is proportional to the exposure received by the dosimeter.

The proposed electret dosimeter is different from other electret dosimeters in both steps 1 and 3.

#### 2.3.4 Other Electret Dosimeters

The first attempt at using an electret to conduct dose measurements was made by Marvin<sup>12</sup> using a carnauba wax electret. Problems of low sensitivity and the instability of the charge signal, both related to the electret material, resulted in limited practical applications. Fabel and Henisch<sup>13</sup> suggested the use of fluorocarbon polymer electrets, with excellent charge storage properties, for dosimetry. Many electret dosimeters were subsequently proposed by Perlman and Unger<sup>14</sup>, Bauser and Ronge<sup>6</sup>, Pretzsch et al<sup>15</sup>, and others. All are similar in that they can be classified as modified parallel—plate or cylindrical ionization chambers, the major modification being the covering of the collecting electrode with a dielectric material — typically a polymer such as Teflon or Mylar — which serves as the electret.

Most electret dosimeters rely on the corona charging process to form the electret. This requires the dismantling of the dosimeter, removal of the polymer, charging of the electret, measurement of the potential above the electret surface to determine the initial charge state, reinsertion of the formed electret into the dosimeter, and reassembly of the dosimeter. In the discharge mode, all electret

dosimeters operate identically with the degree of neutralization of the electret charge layer being proportional to the exposure. For most electret dosimeters, the final charge state is determined by measurement of the potential above the electret surface. This is advantageous in that it is a non-destructive measuring technique but it does require the dismantling of the dosimeter to allow access to the electret surface.

# 2.3.5 The Proposed Electret Dosimeter

The proposed electret dosimeter is similar to others in that it is a modified parallel—plate ionization chamber and thus relies on the neutralization of the charge layer on the electret which covers the collecting electrode as the measuring signal. It is different from others in the manner in which charge is deposited on the electret surface and in the method of acquiring information as to the state of this charge layer.

The electret, or dosimeter, charging technique utilized in the proposed electret dosimeter allows, under ideal conditions, the simultaneous performance of three stages: the formation of the electret, the measurement of the electret's surface charge density, and the verification of the dosimeter's calibration factor. Under non-ideal conditions, to be described in section 4.4, these latter two factors can be determined in the discharging process as well as the measurement of the final surface charge density as the electret is being cleared of all remaining signal. All stages in the regular use of the dosimeter — the charging of the dosimeter, the measurement of the initial charge state, the use in the field, the determination of the final charge state, and the clearing of any remaining signal — are performed in situ and do not involve the disassembly of the dosimeter. In other electret dosimeters, these are all separate steps requiring the dismantling of the dosimeter.

# REFERENCES

<sup>1</sup>G. Hine, G. Brownell, Radiation Dosimetry, (Academic Press Inc., New York, 1956) p.455.

<sup>2</sup>F. H. Attix, Introduction to Radiological Physics and Radiation Dosimetry, (John Wiley and Sons, New York, 1986), p.395.

3Ibid., p.411.

4Ibid., p.418.

<sup>5</sup>Ibid., p.309.

1

6H. Bauser and W. Ronge, "The Electret Ionization Chamber: A Dosimeter for Long-Term Personnel Monitoring", Health Phys., 34, 97-102 (1978).

7G. M. Sessler, Topics in Applied Physics Vol.33: Electrets, 2nd ed. (Springer-Verlag, New York, 1987), p.1.

8O. Heaviside, "Electromagnetic Induction and its propagation. Electrization and Electrification. Natural Electrets", The Electrician, 230-231, 1885.

<sup>9</sup>P. W. Chudleigh, R. E. Collins, G. D. Hancock, "Stability of Liquid Charged Electrets", Appl.Phys.Lett., 23, 211-213, 1973.

<sup>10</sup>G. M. Sessler, Topics in Applied Physics Vol.33: Electrets, 2nd ed. (Springer-Verlag, New York, 1987), p.20.

<sup>11</sup>B. Gross, G. M. Sessler (Ed.), Topics in Applied Physics Vol.33: Electrets, 2nd ed. (Springer-Verlag, New York, 1987), p.268.

12H. B. Marvin, "How to measure radiation with electrets (U.S. Patent No. 2,695,363)", Nucleonics 13, 82-83 (1955)

13G. W. Fabel, and H. K. Henisch, "Polymer Thermoelectret Dosimetry", Phys.

Status Solidi (a) 6, 535-541 (1971).

<sup>14</sup>M. M. Perlman, and S. Unger, "Electron bombardment of electret foils", Appl. Phys. Lett. 24, 579-580 (1974).

<sup>15</sup>G. Pretzsch, B. Dörschel, and B. Leuschner, "Investigation of Teflon Electret Detectors for Gamma Dosimetry", Rad. Prot. Dos. 4, 79-84 (1983).

# CHAPTER 3

#### MATERIALS AND METHODS

#### 3.1 CONSTRUCTION OF THE DOSIMETER

The proposed electret dosimeter is essentially a modified parallel-plate ionization chamber. It consists of two circular electrodes each glued to a flat disk, with a spacer ring keeping a fixed distance between the two disks (see Fig. 3.1). The whole assembly is held together with three nylon screws.

The collecting electrode consists of a circular piece of aluminized polymer (Teflon or Mylar) the aluminum side of which has been etched to electrically insulate the guard from the collector. Several different polymers were tested -110  $\mu m$  Mylar, 76  $\mu m$  Teflon<sup>1</sup>, and 25  $\mu m$  Teflon<sup>2</sup>. Collecting electrode radii of 5 to 19 mm and guard—ring widths of 0 to 19 mm were studied with the sum of the collector radius and guard width never exceeding 21 mm. The polarizing electrode has a diameter of 38 mm or 48 mm and consists of a 10  $\mu m$  aluminum foil.

These electrodes are glued with epoxy to the disk—shaped electrode backing materials. Several different electrode backing materials of 51 mm diameter including 0.8 mm thick bakelite<sup>1</sup>, 1.5 mm fiberglass<sup>3</sup> and 0.75 mm fiberglass were used. The fiberglass boards were originally copper clad circuit boards whose copper had been removed with ferric chloride. Three holes drilled in each disk allow the screws to pass through. These holes are positioned 1.5 mm from the edge of the disk so that the spacer ring is flush with the edge of the disks. The screws thus serve a dual purpose of keeping the spacer rings in position and keeping the two disks and the spacer ring squeezed together. Nylon rather than metal screws are used to prevent the emission of photoelectrons from the screws during irradiation.

Phenolic spacer<sup>1</sup> rings of inner diameter 48 mm and outer diameter 51 mm give a fixed electrode spacing — or air—gap — ranging from 1 mm to 10 mm.

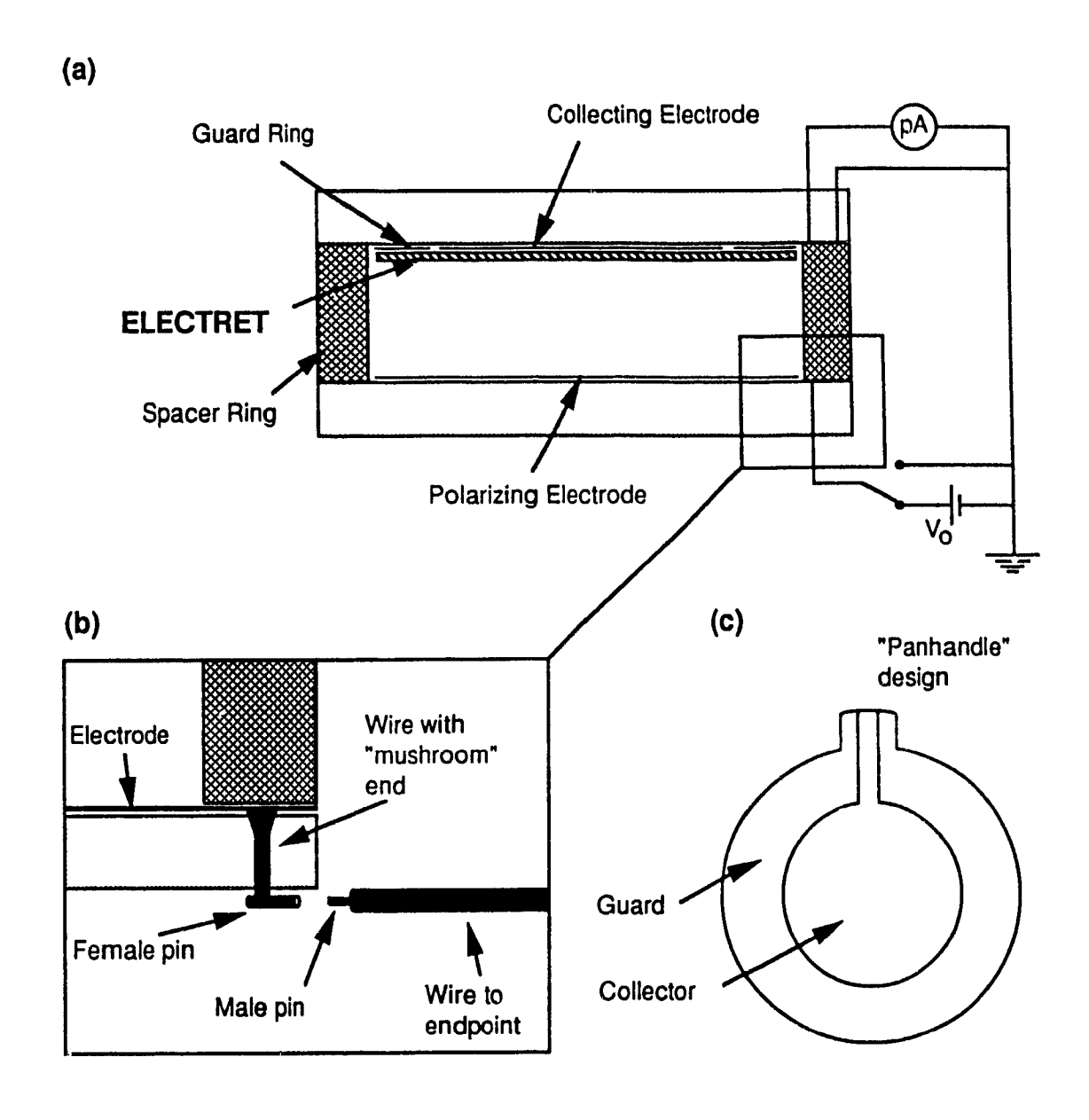


Figure 3.1 (a) Schematic diagram of the electret dosimeter; (b) an expanded view of the electrical connection; (c) a diagram showing the panhandle design of the electrodes.

Standard coaxial cable — type RG 58/U — connects the collecting electrode to the picoammeter and high voltage cable — type RG 59/U — connects the polarizing electrode to the voltage supply.

## 3.2 ELECTRICAL CONTACTS

The electrical contacts connecting the external voltage supply to the polarizing electrode, the picoammeter to the collecting electrode, and the guard-ring to ground consist of a tiny female 60 gauge pin glued with epoxy to the electrode-backing material, and the corresponding male 60 gauge pin soldered to the wire leading either to ground, the external voltage, or the picoammeter. A short length of wire is pushed through a small hole drilled into the electrode-backing material at the edge of the disk. One end of this wire is soldered to the female pin and the other end pushed through the other side of the disk. This end is filed so that the end resembles a mushroom, the head of which is flush with the surface of the disk (see Fig. 3.1(b)). This surface comes into contact with the aluminum electrode itself when the dosimeter is assembled providing the electrical connection from the electrode through the short length of wire, through the female pin, the male pin, and the wire, to the appropriate end-point. This wire is positioned directly under the spacer ring such that the pressure applied between the spacer ring and the electrode backing material provides a solid pressure contact between the head of the wire at the surface of the disk and the electrode itself which extends under the spacer ring.

#### 3.3 ELECTRODE DETAILS

It is necessary to have a small section of each electrode extend under the spacer ring to enable the electrical pressure—contact to be made. This is accomplished by giving the electrodes a type of "panhandle" design (see Fig. 3.1(c))

where a small tab-like extension is added to the circular electrode. This tab then extends under the spacer ring to provide the electrical contact. The presence of this tab causes the area of the collecting electrode to be slightly greater than the product of  $\pi$  and the square of the radius of the collecting electrode. The five different collector radii used were 5, 10, 12.5, 15, and 19 mm with corresponding areas of 0.98, 3.32, 5.00, 7.60, and 12.00 cm<sup>2</sup>.

The collecting electrode presents a problem since it is surrounded by the guard ring. In order to make the electrical connection, an electrical path is provided across the guard ring to give the central collecting electrode access to the outer edge of the disk where the electrical contact can be made (see Fig. 3.1(c)). Note that any etches made to the aluminized polymer are only made to the thin layer of aluminum and not to the polymer itself. If the polymer is accidentally punctured in etching the aluminum, the polymer must be discarded since no part of the collecting electrode can be exposed — not even the very edge for this provides a path for ions to be continually collected.

In a subsequent design, the aluminized polymer and the aluminum polarizing electrode extend completely under the spacer ring around their whole circumference. For accuracy in terms of determining the area of the collecting electrode, the panhandle—designed collecting electrode can be avoided by substituting the electrical pressure contact at the edge of the electrode with a contact made at the center of the electrode. The wire that passes through the fiberglass disk is moved to the center of the dirk and electrical contact is maintained with conductive epoxy<sup>4</sup>. With this design, the panhandle design is not needed thus allowing the collecting electrode to have a perfectly circular shape.

A problem encountered occasionally is an electrical connection between the collecting electrode and the guard ring. Erroneous current readings will register when this occurs since the picoammeter is measuring the current across its two

connected leads. Care must be taken to ensure that no conductive substance bridges the collector/guard etch in the aluminum.

## 3.4 RADIATION SOURCES

-

Several different radiation sources were used to irradiate the dosimeter. A General Electric Maximar 100 superficial therapy unit was used as an X-ray source. It has an exposure rate of 38 mR s<sup>-1</sup> mA<sup>-1</sup> at 90 kVp, 50 cm from the target with the mA ranging from 0 to 6 mA and kVp ranging from 30 to 100 kVp. The half value layer at this kVp was 1.5 mm Al corresponding to an effective beam energy of 26 keV. This source was housed in a 1.5 m × 1.5 m × 1.5 m lead-lined wooden box. A Hewlett Packard Faxitron X-ray source with an exposure rate of 36.7 mR s<sup>-1</sup> mA<sup>-1</sup> at 90 kVp (variable from 10 - 110 kVp), 3 mA fixed, 46 cm from the source was also used. Another source used was a Philips RT250 orthovoltage therapy unit with 4 kVp stations: 100 kVp (HVL of 0.32 mm Cu), 150 kVp (HVL of 0.62 mm Cu), 200 kVp (HVL of 1.3 mm Cu), and 250 kVp (HVL of 2.3 mm Cu). The 250 kVn station was additionally filtered to produce a beam with a HVL of 2.75 mm Cu. An Atomic Energy of Canada Limited Eldorado 6 Cobalt unit was also used. It had a dose rate of 126.4 cGy min<sup>-1</sup> at a depth of 0.5 cm in water, 60 cm from the source, with a  $10 \times 10 \text{ cm}^2$  field.

The exposure rate was measured at low energies (on the Maximar 100 and the Faxitron) with a Keithley Digital Dosimeter Model 35055 and a 15 cc parallel—plate ion chamber; and at intermediate energies (on the orthovoltage unit) with a Farmer Dosimeter Reader Model 2570 and a 0.6 cc cylindrical Farmer chamber. The Cobalt unit's calibration factor was used. It had been measured with a 0.6 cc cylindrical Farmer chamber at a depth of 0.5 cm in phantom.

The mean effective energy of the radiation beam was determined by measuring the half—value layer and calculating the mass attenuation coefficient using the relation<sup>5</sup>,

$$\mu = (\ln 2)/HVL \tag{3.1}$$

The photon energy corresponding to this mass attenuation coefficient for the attenuating material used would then be determined from tables of  $\mu$  vs. photon energy.

## 3.5 MEASUREMENTS

The experimental set—up involved placing the electret dosimeter under the radiation source and connecting the three wires to the dosimeter — the polarizing electrode to the external voltage supply (a Keithley 245 high voltage supply (0 — 2000 V)), the collecting electrode to the picoammeter (a Keithley 35617 programmable electrometer), and the guard—ring to ground. Data acquisition was performed with an IBM compatible personal computer through an IEEE—488 interface with the picoammeter. To charge the electret, the external voltage supply would be switched on and the dosimeter irradiated. The computer acquired the current reading from the picoammeter once every 0.323 seconds for as many points as were needed until the charging process was complete. Signal analysis was then performed on the computer.

# REFERENCES

<sup>1</sup>Commercial Plastics & Supply Corp., Montreal, Quebec.

<sup>2</sup>Sheldahl Inc., Northfield, Minnesota.

<sup>3</sup>Pulsar Circuits Inc., Dollard Des Ormeaux, Quebec.

4Hysol Canada Inc., Electronic Chemicals Division, Scarborough, Ontario.

<sup>5</sup>H. E. Johns, J. R. Cunningham, *The Physics of Radiology*, (Charles C Thomas, Springfield, Illinois, 1983), p.137.

#### **CHAPTER 4**

# THE ELECTRET DOSIMETER

# 4.1 INTRODUCTION

The basic methodology specific to the use of the proposed electret dosimeter is as follows:

- 1. A charge,  $q_i$  is deposited on the polymer surface. This is accomplished in the dosimeter-charging process by applying a potential across the electrodes and irradiating the dosimeter (to be discussed in section 4.2.2).
- 2. The dosimeter is then used in the field with  $q_i$  being depleted by an amount,  $q_x$ , due to exposure to radiation.
- 3. The remaining charge,  $q_f$ , on the polymer surface is then determined directly by discharging the dosimeter through irradiation and measuring the remaining charge as it is being neutralized (section 4.2.3).
- 4.  $q_x$  is then calculated  $(q_x = q_i q_f)$  and related to the exposure received by the dosimeter through the calibration factor which is valid for a given exposure range.

# 4.2 DOSIMETER CHARGING/DISCHARGING BY RADIATION—INDUCED AIR—IONIZATION

# 4.2.1 Introduction

The dosimeter charging/discharging method used here was first described by Fallone and Podgorsak<sup>1</sup>. It relies on the use of indirectly ionizing radiation -X or  $\gamma$  radiation - to create charge carriers in air, and the use of a potential difference between the electret and an opposing electrode to collect these charge carriers on the

electret's surface. This method is thus very similar to the corona charging technique where a large potential difference between the electret and a point—shaped electrode, resulting in an inhomogeneous electric field, produces a discharge in air; hence the creation of the charge carriers, and the collection of the charge carriers due to the applied potential.

# 4.2.2 Dosimeter Charging

Consider a collecting electrode covered with a dielectric material and a polarizing electrode separated by a distance a (see inset to Fig. 4.1(a) under "Charging"). With the collecting electrode held at ground, a voltage applied to the polarizing electrode creates an electric field,  $\mathbf{E}_a$ , in the volume between X or  $\gamma$  radiation passing through this volume results in the the electrodes. production of charge carriers due the ionizing nature of the radiation. These charge carriers drift toward the electrodes under the influence of the field  $\mathbf{E}_a$  with those moving towards the collector becoming trapped on the insulating dielectric material (in this case a polymer) that covers this electrode. gathering on the polymer surface induces a flow of compensation charge onto the collector from ground through an electrometer which is used to measure this signal. If the voltage on the polarizing electrode is high enough, the chamber will be in saturation - a negligible amount of recombination of charge carriers will occur — and a saturation current  $I_{sat}$  will flow (as indicated in Fig. 4.1(a)). This would be exactly the same current one would measure with a standard parallel-plate ionization chamber of the same dimensions. However, with the polymer covering the collecting electrode, this current does not persist, as it would in an ionization chamber. As the charge layer on the polymer surface builds up, the field produced by the charge layer,  $E_{\sigma}$ , begins to cancel the field due to the voltage on the polarizing electrode until the cancellation is large enough to bring the

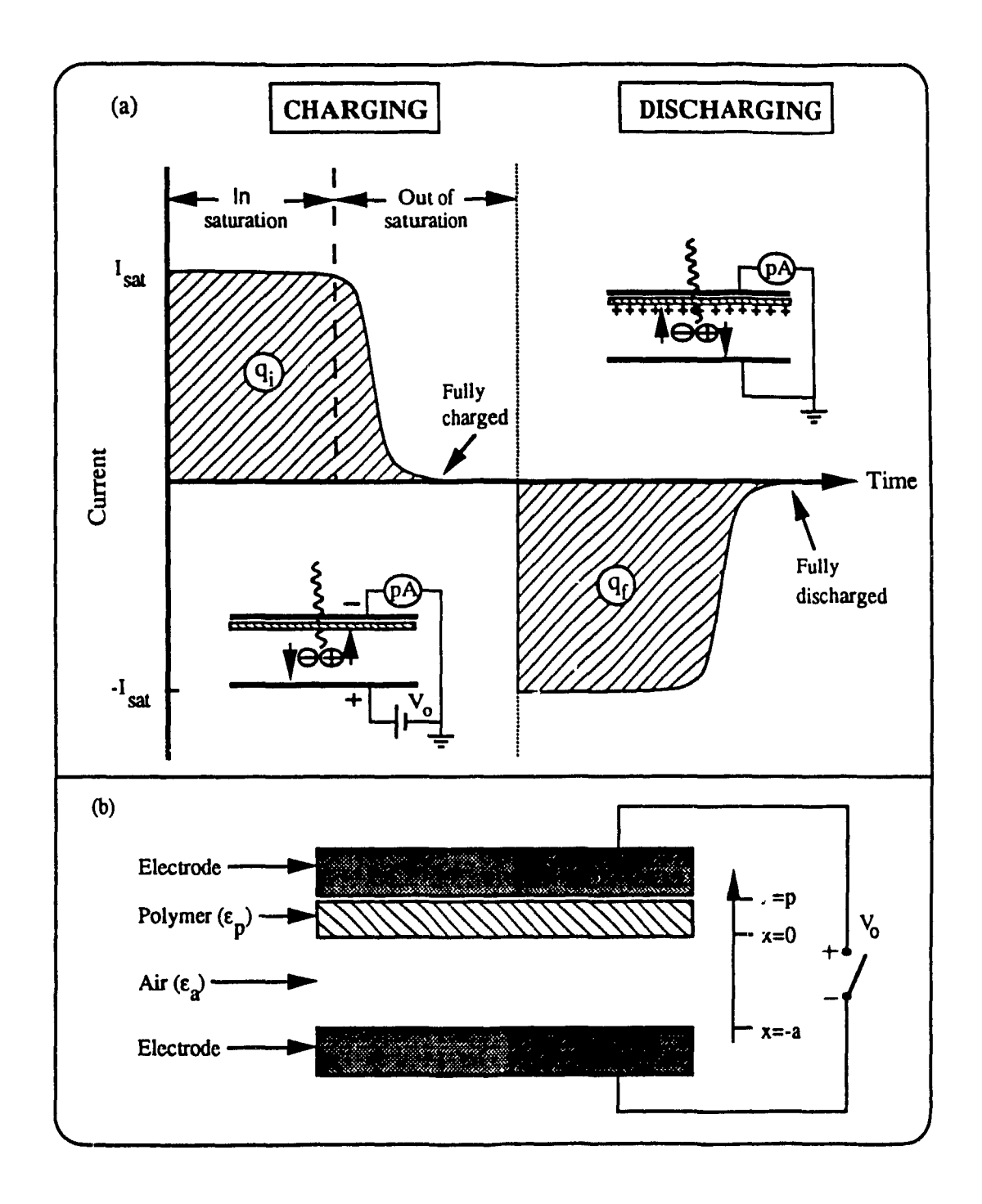


Figure 4.1 (a) Schematic showing the measured current in saturation and out of saturation for both the charging of the dosimeter and the discharging; (b) diagram of the electrode/polymer/air/electrode interface.

chamber out of saturation. At this time the measured current drops exponentially. When the field produced by the electret charge layer exactly cancels the field produced by the voltage on the polarizing electrode ( $\mathbf{E}_{\sigma} = \mathbf{E}_{a}$ ), there will be no more net movement of charge carriers and the measured current will be zero. At this point, the dosimeter is fully charged — the electret is formed.

This technique allows great control over the electret forming process. The polarity of the applied potential determines the sign of the charge carriers collected on the electret surface — a positive potential on the polarizing electrode results in the collection of positive charge carriers on the electret surface and a negative potential results in negative charge carriers being collected. The amount of charge deposited on the electret surface is directly related to the value of the potential difference.

The relationship between the voltage measured at the electret surface and the surface charge density can be obtained for the specific geometry in question from the general equations given by Sessler<sup>2</sup>. Consider a charge layer of charge density  $\sigma$  at x=0 with a dielectric extending to x=p, where p is the thickness of the dielectric (of dielectric constant  $\epsilon_p$ ), and an electrode at x=p. Another electrode is situated at x=-a, where a is the thickness of the air-gap (of dielectric constant  $\epsilon_a$ ) between the surface of the dielectric and the opposite electrode (see Fig. 4.1(b)). The permittivity of free space is denoted by  $\epsilon_o$ . Gauss' law for the electric displacement applied to the x=0 interface gives,

$$-\epsilon_a E_a + \epsilon_p E_p = \sigma/\epsilon_o \tag{4.1}$$

From Kirchoff's second law,

$$V_o + aE_a + pE_p = 0 (4.2)$$

Equation 4.1 is solved for  $E_p$  and substituted into equation 4.2 to obtain,

$$E_{a}(a/\epsilon_{a} + p/\epsilon_{p}) = -V_{o}/\epsilon_{a} - p\sigma/\epsilon_{o}\epsilon_{p}\epsilon_{a}$$
 (4.3)

The potential at the dielectric surface (x = 0) due to  $\sigma$  with  $V_o = 0$  is,

$$V = -aE_a = \frac{\sigma}{\epsilon_o(\epsilon_p/p + \epsilon_a/a)}$$
 (4.4)

which for  $a \gg p$  becomes,

$$V = \sigma p / \epsilon_o \epsilon_p \tag{4.5}$$

This is the basic equation relating the potential at the electret surface to the charge density on the electret.

The dosimeter charging process was described theoretically by Fallone and Podgorsak<sup>3</sup> using the laws of Gauss and Kirchoff and a hyperbolic expression for the saturation curve. At the start of the charging process, no charge is present on the dielectric surface hence the electric field in the sensitive volume is due solely to the external voltage  $V_o$ . Solving equation 4.3 for  $E_a$  with  $\sigma=0$ ,

$$E_a(0) = -V_o \epsilon_p / (p \epsilon_a + a \epsilon_p) \tag{4.6}$$

At any time during the charging process, the effective electric field  $E_{\it eff}$  in the sensitive volume is the sum of the field due to the applied voltage and the field due to the developing charging layer:

$$E_{eff}(t) = E_a(0) - E_{\sigma}(t) = \frac{(p\sigma(t)/\epsilon_0) - V_0 \epsilon_p}{p\epsilon_a + a\epsilon_p}$$
 (4.7)

The saturation curve can be approximated by 4,

$$j/j_{sat} = \tanh(E/E^*) \tag{4.8}$$

where j is the measured current density,  $j_{sat}$  is the saturation current density, E is the applied electric field, and  $E^*$  is the extrapolated electric field, the field at which the collection efficiency would equal unity if the initial linear relationship between the collection efficiency and E, exhibited at small fields, held for all electric fields. Combining<sup>3</sup> equations 4.7 and 4.8 and solving for j,

$$j(t) = j_{sat} \exp[(t_o - t)/\tau] \{1 + \exp[2((t_o - t)/\tau]\}^{-1/2}$$
(4.9)

where  $\tau$  is the electret relaxation time, and  $t_o$  is the electret characteristic polarization time.  $\tau$  and  $t_o$  are defined below,

$$\tau = \beta E^* / j_{sat} \tag{4.10}$$

$$t_o = \tau \ln \sinh[E_a(0)/E^*]$$
 (4.11)

where  $\beta = \epsilon_o(p\epsilon_a + a\epsilon_p)/p$  and  $E_a(0)$  is the initial applied electric field.

1

This theory predicts a charge—up current density which begins with a constant saturation current density that remains for a time determined by the value of the applied external voltage followed by a quick drop to a current density of zero, as seen in Fig. 4.1(a). The main assumption in this theory is that the electric field lines are uniform and parallel across the sensitive volume.

# 4.2.3 Dosimeter Discharging

In the discharging process, the applied voltage is removed from the polarizing electrode and the two electrodes are shorted. Now the electric field in the sensitive volume is due solely to the charge layer on the electret. With irradiation, the charge carriers produced in the sensitive volume that are of opposite sign to those on the electret surface are attracted to this surface and begin to neutralize the charge layer (see inset to Fig. 4.1(a) under "Discharging"). Again a compensation current is measured by the electrometer however the current flows in the opposite direction to the charging current, thus the negative current in the diagram. Once again saturation conditions exist, hence the saturation current,  $-I_{sat}$ , flows until the charge layer is depleted to a point where saturation conditions do not exist and the current begins to drop. Finally the charge layer is fully depleted and the current drops to zero since there is no electric field to cause the movement of charge carriers. At this point the discharge process is complete.

In order to retain simplicity and accuracy in calibrating the electret dosimeter, it is necessary for the the dosimeter to remain in saturation during use. This condition is satisfied for surface charge densities greater than  $\sigma_{sat}$ , the minimum surface charge density needed to provide saturation conditions, and less than  $\sigma_{prop}$ , the surface charge density at which gas multiplication conditions set in. While the chamber is in saturation, the exposure is linearly related to the measured charge—density. Once out of saturation, the linearity no longer holds. Hence, for each dosimeter configuration, there are limits on the maximum and minimum surface charge densities necessary to provide saturation conditions.

The minimum charge density necessary to maintain saturation conditions can be calculated with the aid of Mie's<sup>5</sup> equation which relates the applied voltage across the chamber V and the collection efficiency (f),

$$V = 0.828 RI_{sat} \sqrt{f/(1-f)}$$
, for  $f > 0.67$  (4.12)

where  $I_{sat}$  is the current measured at saturation, and R is the ohmic resistance of the ionized gas between the measuring electrodes at very weak strengths given by  $^6$ ,

$$R = \frac{a^{3/2} (\alpha_o/e)^{1/2}}{(AI_{sat})^{1/2} (\mu_1 + \mu_2)}$$
(4.13)

a is the air-gap, A is the area of the collecting electrode,  $\alpha_0$  is the the volume recombination coefficient, e is the electron charge, and  $\mu_1$  and  $\mu_2$  are the mobilities of positive and negative charge carriers, respectively.

For a collection efficiency of 99 %, V is given by

$$V = 8.238 RI_{sat}$$
, for  $f = 0.99$  (4.14)

Substituting equation 4.5,

Ţ

$$\sigma_{sat} = \xi R I_{sat} \tag{4.15}$$

where  $\xi = 8.238 \epsilon_0 \epsilon_p/p$ . This gives the minimum charge density  $\sigma_{sat}$  required to maintain saturation conditions (99 % collection efficiency).

An upper limit on the charge density is necessary to keep the dosimeter out of the gas multiplication region where the charge carriers gain enough energy in their acceleration toward the electrode to create additional ionizations. At atmospheric pressure, the minimum field strength  $E_{prop}$  required for the onset of gas multiplication in air is estimated at 10 kV/cm. Using equation 4.5,  $\sigma_{prop}$ , the maximum surface charge density on the electret before gas multiplication conditions set in, is,

$$\sigma_{prop} = E_{prop} a \epsilon_o \epsilon_p / p \tag{4.16}$$

As long as saturation conditions exist (i.e. for  $\sigma_{sat} < \sigma < \sigma_{prop}$ ), the rate of charge generation in the whole sensitive volume, and hence the rate at which the surface charge density on the electret is being depleted, is given by 8,

$$j_{sat} = e \dot{n} a \tag{4.17}$$

where e is the charge of the electron,  $\dot{n}$  is the number of ions produced in the sensitive volume per unit time per unit volume, and a is the distance between the electrodes. Converting ion production rate to exposure rate using the relation,

$$e\dot{n} = \kappa \dot{X} \tag{4.18}$$

where  $\kappa = 3.33 \times 10^{-10}$  C cm<sup>-3</sup> R<sup>-1</sup> (neglecting possible charge creation due to photoemission – to be discussed in section 4.3) and  $\dot{X}$  is the exposure rate, the saturation current density is,

$$j_{sat} = \kappa a \dot{X} \tag{4.19}$$

or equivalently,

$$\sigma(X) = \sigma_0 - \kappa a X \tag{4.20}$$

where  $\sigma_o$  is the initial charge density of the electret. This linear relationship between the reduction in the electret's surface charge density and the exposure is used as the measuring signal.

In order to appreciate the necessity of the maintenance of saturation conditions, it is instructive to determine the rate which the charge density is decreased when the surface charge density on the electret is not sufficient to produce saturation conditions.

If saturation conditions do not exist, the recombination of ions produced in the sensitive volume causes the relationship between the reduction in surface charge density and exposure to be nonlinear. This can be seen by considering the lifetime of the ion to be  $\eta$ . The change in surface charge density per unit time<sup>9</sup> is,

$$d\sigma/dt = -e\dot{n}\eta v \tag{4.21}$$

where v is the group velocity of the ions of mobility  $\mu$  in an electric field E,

$$v = \mu E = \mu(\sigma/\epsilon_0) \tag{4.22}$$

since  $E = \sigma/\epsilon_0$  for an electret with an opposing parallel electrode. Substituting equation 4.22 into 4.21,

$$d\sigma/dt = -(ei\eta\mu/\epsilon_0)\sigma \tag{4.23}$$

Solving for  $\sigma$ ,

1

100

$$\sigma(t) = \sigma_o \exp[-(e\dot{n}\mu/\epsilon_o)\eta t] \tag{4.24}$$

Substituting equation 4.18 into 4.24,

$$\sigma(X) = \sigma_0 \exp[-(\mu/\epsilon_0)\eta \kappa X] \tag{4.25}$$

The reduction in surface charge density on the electret is thus exponential with exposure under non-saturation conditions. This is due to the fact that in order to be collected, the ions must be produced no further than a distance L from the electret, where  $L = v\eta$  and L < a. Ions produced beyond this distance recombine and do not contribute to the signal. As the charges on the electret surface are neutralized by the collected charges, the electric field E produced by the charge layer is decreased, causing the volume from which ions can be collected before recombining to decrease, thus giving rise to the exponential relationship.

# 4.2.4 The Charge/Discharge Curve

The electret charge/discharge curve is the standard dataset acquired for each different dosimeter configuration. With it one can deduce essential information such as the saturation current for a given exposure rate, the maximum exposure to which the dosimeter can be exposed before saturation conditions no longer exist, and a wealth of other information which will be described in the next few sections. It is therefore one of the basic diagnostic tools for analyzing the dosimeter's performance. Knowledge of the dosimeter's response as it is being exposed to radiation is indispensable since it allows verification of the electret's charge density state as a continuous function of time.

Normally dosimeter—charging would not be followed by dosimeter—discharging. The standard progression of events would be: charging of the dosimeter, exposure in the field, and finally discharging of the dosimeter. These last two steps can be combined for dosimeter—analysis purposes. All dosimeter charging was performed with a negative polarity on the applied voltage (see section 4.6.5).

A charge/discharge curve is shown in Fig. 4.2(a). The dosimeter configuration used to acquire this curve was as follows: a collecting electrode radius c of 15 mm, a guard—ring width q of 9 mm, a polarizing electrode radius of

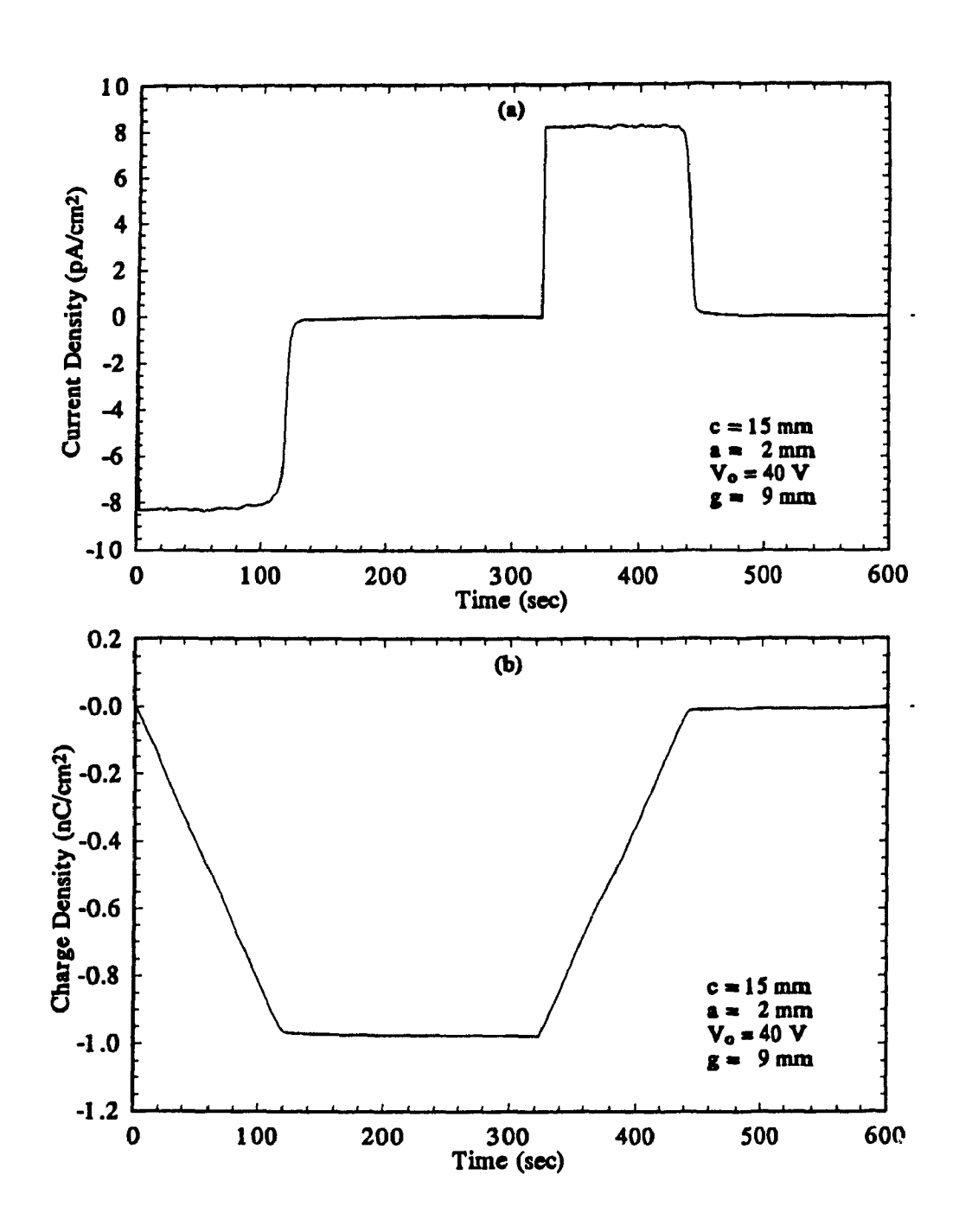


Figure 4.2 A charge/discharge curve plotting (a) current density versus time and (b) charge density versus time for a 110  $\mu$ m Mylar electret and an exposure rate of 0.11 R s<sup>-1</sup> at 90 kVp (effective energy 26 keV).

19 mm, an air—gap a of 2 mm, and a charging voltage of -40 V (i.e.  $V_o=40$  V). Irradiation of the dosimeter began before data acquisition started. At time t=0 seconds, an external voltage was applied to the polarizing electrode and a saturation current density of -8.25 pA/cm<sup>2</sup> began to flow through the picoammeter. This current stayed constant until at t=105 sec, the net electric field (sum of the fields due to the applied potential and the developing charge layer) decreased to the point that it was not large enough to result in saturation conditions, and the current began to decrease until at t=122 sec, the net electric field reached zero — without an electric field there can be no net movement of charge carriers in the sensitive volume, hence no current. After removing the external voltage and grounding the polarizing electrode at t=324 sec a saturation current density of 8.25 pA/cm<sup>2</sup> flowed until t=429 sec when the current decreased to zero once the electret charge layer was fully depleted.

From Fig. 4.2(a), it is evident that saturation conditions exist for almost the entire discharge process. Apparently a very small charge density on the electret is sufficient to retain saturation conditions. This can be verified using equation 4.14. For the Mylar polymer used,  $\epsilon_p = 3.2$  and  $p = 110~\mu\text{m}$ , with  $\epsilon_0 = 8.85 \times 10^{-12}~\text{C}^2$  N<sup>-1</sup> m<sup>-2</sup> so that  $\xi = 2.12 \times 10^{-6}~\text{C}^2~\text{N}^{-1}~\text{m}^{-3}$ . To calculate R, typical values for some of the parameters are used <sup>10</sup>:  $\alpha_0 = 1.95 \times 10^{-12}~\text{m}^3~\text{s}^{-1}$ ,  $e = 1.602 \times 10^{-19}~\text{C}$ ,  $\mu_1 = 1.3 \times 10^{-4}~\text{m}^2~\text{V}^{-1}~\text{s}^{-1}$ ,  $\mu_2 = 1.8 \times 10^{-4}~\text{m}^2~\text{V}^{-1}~\text{s}^{-1}$ . A for this collector is  $7.602 \times 10^{-4}~\text{m}^2~\text{and}~I_{sat} = 62.7~\text{pA}$  for a = 0.002~m giving a value for R of 4.61 ×  $10^9~\Omega$ . The product of  $\xi$ , R, and  $I_{sat}$  is  $\sigma_{sat}$  the charge density necessary to maintain saturation for this dosimeter configuration, and is equal to 0.061 nC cm<sup>-2</sup> or equivalently a voltage of 2.37 V. From the plot of charge versus exposure (Fig. 4.2(b)), it is seen that this value corresponds well with the actual value of the charge density at which saturation conditions were lost (at t = 438~seconds).

### 4.3 CALIBRATION

1

N. C.

The magnitude of the charge removed from the electret per incident unit of exposure is the basic calibration factor which must be determined. This factor k allows one to calculate the exposure knowing the difference in charge states on the electret before and after the exposure. Ideally it would be calculated from equation 4.20 and would thus be equal to  $\kappa a$ . This neglects any charge collected due to the ionization of air by photoelectrons backscattered into the sensitive volume from the material surrounding the sensitive volume. Thus the measured signal is due to two components,

$$j_{sat}(a) = j_{sat}^{air}(a) + j_{sat}^{p}(a)$$
 (4.26)

where  $j_{sat}(a)$  is the measured saturation current density, the linear function  $j_{sat}^{air}(a)$  is the saturation current density due to direct interactions of photons with air given by equation 4.19, and  $j_{sat}^{p}(a)$  is the saturation current due to photoelectrons backscattered from the polarizing electrode into the sensitive volume described by the empirical relationship<sup>11</sup>,

$$j_{sat}^{p}(a) = \lambda' \dot{X} \nu [1 - \exp(3a/a_r)]$$
 (4.27)

where  $\lambda'$  is  $1.33 \times 10^{-6}$  C R<sup>-1</sup> cm<sup>-2</sup>,  $\nu$  is the efficiency for production of backscattered electrons for a material of atomic number Z and photon energy  $E_{\nu}$ , a is the air-gap and  $a_r$  is the photoelectron range for incident photon energy  $E_{\nu}$ .

From equation 4.26, incorporating equations 4.19 and 4.27, the response of the dosimeter to irradiation is thus,

$$j_{sat}(a) = \dot{X}[\kappa a + \lambda' \nu \{1 - \exp(3a/a_r)\}]$$
 (4.28)

The factor relating the saturation current density to the exposure rate, or alternatively the surface charge density to the exposure, is,

$$k' = \kappa a + \lambda' \nu [1 - \exp\{3a/a_r(E_{\nu})\}]$$
 (4.29)

and the calibration factor k which relates the total charge on the electret to the exposure is,

$$k = k'A \tag{4.30}$$

where A is the area of the collecting electrode. In practice this expression is evaluated by measuring the electret dosimeter's saturation current when exposed to an exposure rate measured with a standard calibrated ion chamber whose calibration factor is traceable to national standards:

$$k = \frac{I_{sat}}{\dot{X}} \tag{4.31}$$

The dosimeter charge/discharge curve from Fig. 4.2(a) was obtained with an exposure rate of  $0.11 \text{ R s}^{-1}$ . For this dosimeter configuration, with a collector area of 7.6 cm<sup>2</sup>, the calibration factor is  $0.57 \text{ nC R}^{-1}$ . Alternatively, k can be determined by evaluating the slope of the charge versus exposure plot (i.e. the integral of the current curve shown in Fig. 4.2(b)). Note that the saturation current for the charging process is the same as that for the discharging process thus the calibration factor for this dosimeter configuration could be verified during the charging process.

The linearity of k with exposure rate was examined (Fig. 4.3) and found to be excellent. This was expected since the dosimeter is of the basic ion chamber

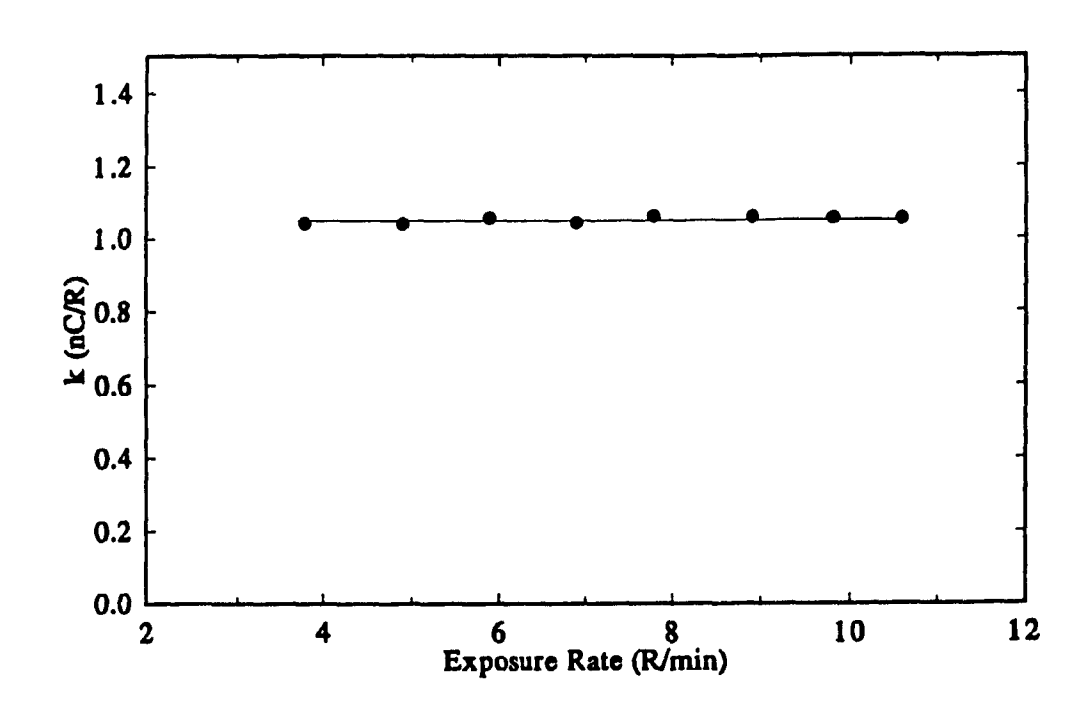


Figure 4.3 The calibration factor as a function of exposure rate for a dosimeter with a 110  $\mu$ m Mylar electret, an air—gap of 3.2 mm, and a collector radius of 12.5 mm at 90 kVp (effective energy: 26 keV).

design. An exposure rate dependence will occur at very high exposure rates, as for regular ionization chambers, where recombination effects might become significant. This situation is not normally encountered in personnel dosimetry.

An example of the diagnostic use of the charge curve is seen in Fig. 4.4. It can be seen that in the charging process, the measured current never decreased to zero. This indicated that there was some portion of the collecting electrode that was not covered with polymer, thus providing a path for the continual collection of charge carriers — just as in a regular ion chamber.

#### 4.4 SENSITIVITY

The sensitivity of the dosimeter - i.e. the factor k - can be altered by varying the amount of charge collected per incident unit of exposure. This seems artificial since the amount of charge produced per unit of exposure is fixed. The unit of exposure is defined as the absolute value of the total charge, dQ, of the ions of one sign produced in air when all of the electrons liberated by photons in a volume element of air of mass, dm, are completely stopped in  $air^{12}$  with its special unit, the roentgen, being defined as:

$$1 R = 2.58 \times 10^{-4} C \text{ kg}^{-1} \text{ of air}$$
 (4.32)

As is evident, the total charge produced per unit exposure is fixed for a given mass of air. By increasing the mass of air from which ions are collected, the total charge collected will be greater but the exposure remains the same. Effects of the dosimeter wall on attenuation of the x-ray beam and photoelectrons backscattered into the sensitive volume from the polarizing electrode can be accounted for by calibrating the electret dosimeter with an absolute dosimeter, therefore the response

Figure 4.4 A charge/discharge curve of current density versus time for a 110  $\mu m$  Mylar electret showing the effect of a collector not fully covered with polymer.

A ....

of the electret dosimeter per unit absolute exposure can be varied. The calibration factor relates the measured relative reading with the absolute exposure.

The response of the electret dosimeter can be altered by varying the size of the sensitive volume, as seen in the equations defining the calibration factor (4.29 and 4.30). Altering the size of the air—gap or the radius of the collecting electrode will affect the sensitivity since a larger sensitive volume results in a greater number of charge carriers being collected and hence a larger calibration factor.

Fig. 4.5 shows a discharge curve for the same dosimeter as Fig. 4.2, except the air-gap has been increased to 6 mm. The calibration factor is now 1.40 nC  $\rm R^{-1}$  and the sensitivity is much greater. The saturation current density for the charging process is seen to be different from that of the discharging process:  $j_{sat}$  for charge-up is -18.6 pA/cm<sup>2</sup> and  $j_{sat}$  for discharging is 20.2 pA/cm<sup>2</sup>. The reason for this, as well as the cause of the distortion of the charge-up curve, will be explained in sections 4.5.2 and 5.4. For small air-gaps, it has been shown that the two saturation currents are equal. Differences between the charge-up and the discharge current curves arise when the size of the air-gap is increased above a certain level. However, in use, the electret dosimeter is always in the discharge mode. It is thus more important to analyze the characteristics of the discharge curve, rather than those of the charge-up. Hence, any future reference to saturation currents or calibration factors imply those of the discharge mode rather than the charge-up mode unless explicitly stated otherwise.

Current curses were acquired for air—gaps ranging from 1.5 mm to 9.6 mm. A plot of the calibration factor vs air—gap (Fig. 4.6) shows the increase in sensitivity with increasing air—gaps. As can be seen from the graph, however, this relationship is not a linear one: a doubling of the air—gap, and hence the sensitive

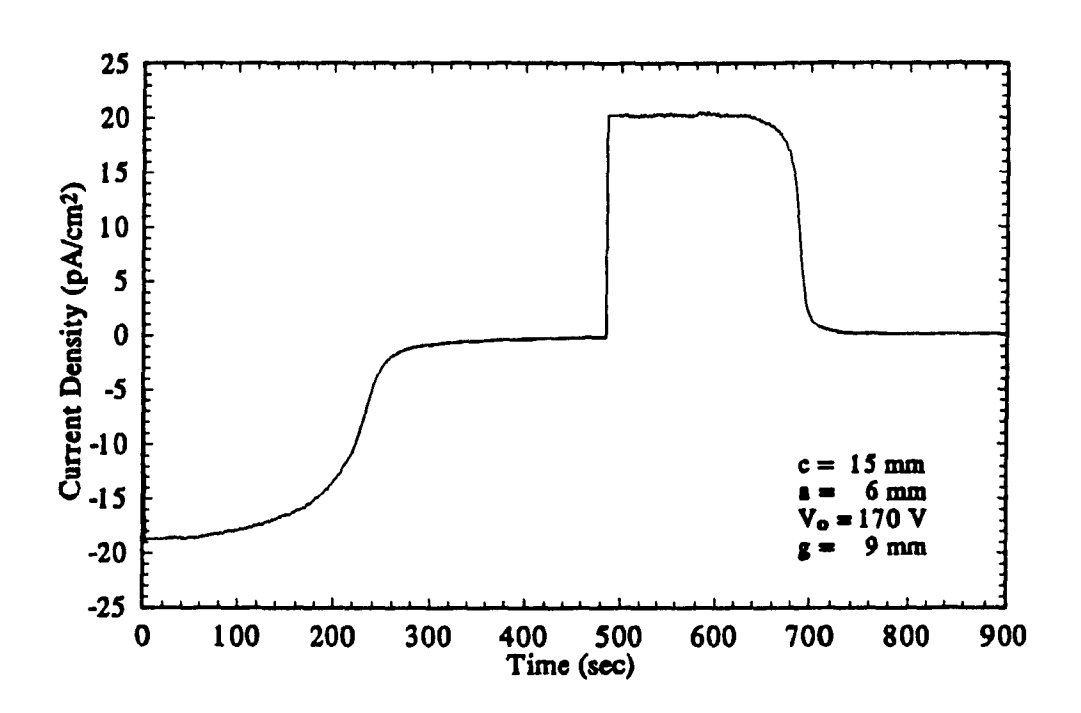


Figure 4.5 A charge/discharge curve of current density versus time for the same dosimeter as Fig. 4.2 except for the increased air—gap.

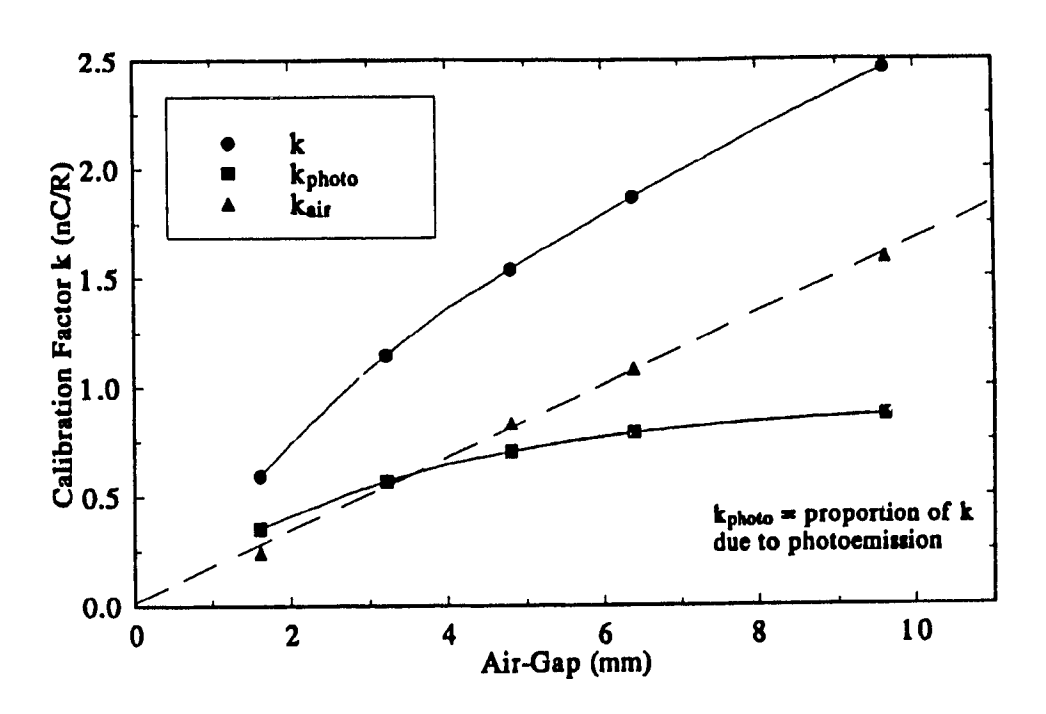


Figure 4.6 The calibration factor k as a function of the air—gap a for a 90 kVp x—ray beam and a 110  $\mu$ m Mylar electret showing the proportion of k due to photoemission from the polarizing electrode,  $k_{photo}$ , and to direct x—ray interactions with air,  $k_{air}$ .

volume, does not produce a doubling of the saturation current. The reason for this is twofold: the first involves the contribution of the photoemission current due mainly to photoelectrons emitted from the polarizing electrode, and the second is related to the problems encountered at large air—gaps, to be discussed further in section 5.2.

The exposure rate is calculated as follows,

$$\dot{X}_{calc} = I_{sat}/(m_{air}\chi) \tag{4.33}$$

where  $m_{air}$  is the mass of air from which ions are collected and  $\chi$  is given by equation 4.32. With an air—gap of 0.2 cm, a collector radius of 1.9 cm, and  $I_{sat}$  of 104 pA, the calculated exposure rate exceeded the exposure rate measured with a calibrated ion chamber (0.11 R s<sup>-1</sup>) by 34 % for a 90 kVp X—ray beam. This difference arises mainly from the added contribution to the collected charge from the photoemission current due to the polarizing electrode, as discussed in section 4.3, as well as problems associated with determining the mass of air from which ions were collected — not always equal to the product of the physical size of the volume between the electrodes and the density of air.

The number of photoelectrons backscattered into the sensitive volume is dependent on the atomic number of the material comprising the polarizing electrode or other material surrounding the sensitive volume  $Z_s$  and the energy of the incident photon  $h\nu$  since the cross section per electron for the photoelectric effect is proportional 13 to  $Z^{3.8}$  for low Z materials and  $Z^3$  for high Z materials, and to  $(h\nu)^{-3}$ . By increasing  $Z_s$ , the sensitivity can be increased dramatically, however a large energy dependence is introduced. As will be discussed in section 6.2, it is preferable to keep  $Z_s$  close to the effective atomic number of air.

By subtracting the portion of the signal due to photoemission, the linear relationship between k and a which is due to the direct interaction of photons with air results. This can be done using equation 4.27. With  $a_r = 1$  cm for the 90 kVp beam used, the measured current density is expected to become linear at an air—gap equal to this range since the current due to photoemission decreases exponentially with increasing air—gap. The amount of charge collected per roentgen for the total measured signal, the photoemission portion, and the charge collected due to direct photon interactions with air is plotted in Fig. 4.6 showing the linear relationship which results when the photoemission current is subtracted.

The contribution to the total signal due to photoemission should be much reduced at higher photon energies due to the energy dependence of the cross section for the photoelectric effect. A plot of k vs. a for a Cobalt-60 unit as the radiation source is shown in Fig. 4.7. The linearity between the two factors is much better. The difference between the calculated exposure rate (for a 0.2 cm air-gap, a 1.9 cm radius collector and  $I_{sat} = 190$  pA) and the measured exposure rate (0.272 R s<sup>-1</sup>) is much improved with a 0.7 % difference between the two values.

## 4.5 EXPOSURE RANGE

## 4.5.1 Maximum Exposure

The exposure range of the dosimeter is limited by the requirement that the surface charge density of the electret be large enough to produce saturation conditions. Thus the dosimeter can only undergo an exposure  $X_{max}$  before the surface charge is depleted to the point where this minimum surface charge density is reached. If the initial surface charge density  $\sigma_i$  were increased, this maximum exposure is correspondingly increased since a larger exposure would now be needed to deplete the increased surface charge. One method of increasing the initial surface charge density is to increase the voltage applied to the polarizing electrode during

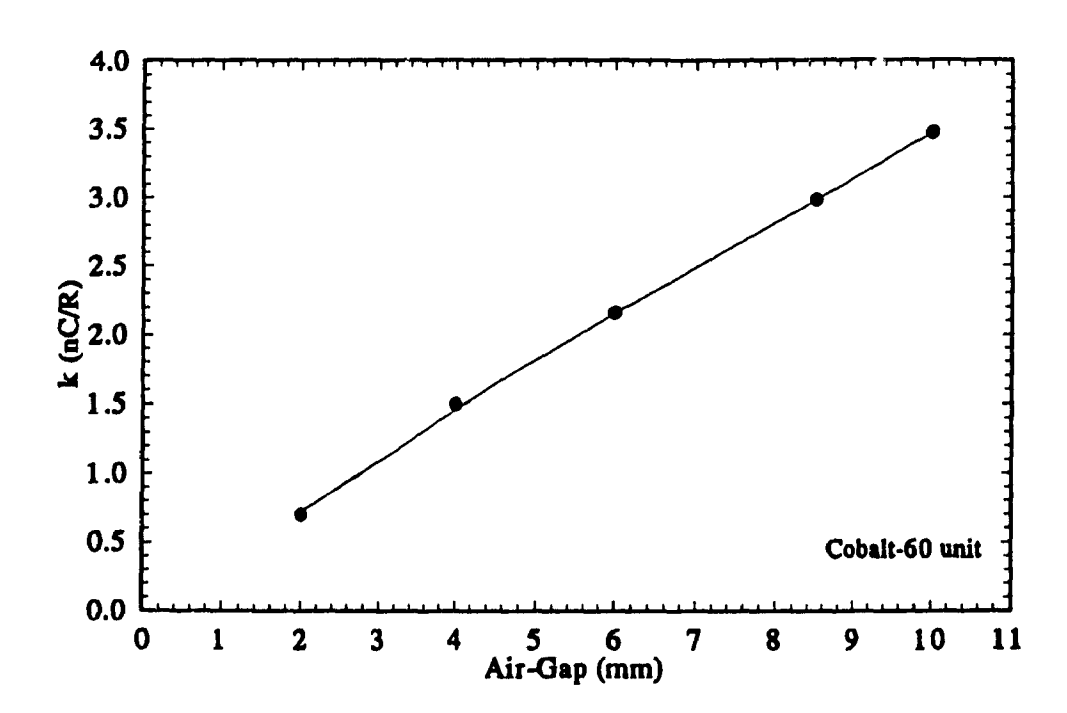


Figure 4.7 The calibration factor k as a function of the air—gap a for a Cobalt—60 radiation source (110  $\mu$ m Mylar electret and a 19 mm collector radius).

the electret charge—up process. A larger surface charge density is reached at the end of the formation process in order to counter this elevated applied voltage.

The surface charge density  $\sigma$  on the polymer surface is given by equation 4.5. Rearranging,

$$\frac{\epsilon_0 \epsilon_p}{p} = \frac{\sigma}{V_0} \tag{4.34}$$

it is clear that for a given polymer thickness, there is a constant,  $\lambda$ , where

$$\lambda = \frac{\epsilon_0 \epsilon_p}{p} \tag{4.35}$$

which gives the charge density per volt on the electret. Dividing  $\lambda$  by k', the number of roentgen per volt is determined for that electret:

$$\frac{\lambda}{k'} = \phi \tag{4.36}$$

where k' is given by equation 4.29. The exposure required to deplete the electret of all charge  $X_{depl}$  is thus,

$$X_{depl} = \phi V_o \tag{4.37}$$

where  $V_o$  is the voltage to which the dosimeter was initially charged.

This exposure would be sufficient to totally deplete the electret charge layer and hence it is not the maximum useful exposure  $X_{max}$  — the maximum exposure that the dosimeter can undergo while still remaining in saturation — mentioned earlier. The maximum useful exposure is less than the exposure required to fully

deplete the charge layer and is simply the difference in charge densities between the initial charge density  $\sigma_i$  and the minimum charge density required to maintain saturation conditions,  $\sigma_{sat}$  divided by the reduction in charge density per unit exposure,

4

-

$$X_{max} = \frac{\sigma_i - \sigma_{sat}}{k'} \tag{4.38}$$

where  $\sigma_{sat}$  is given by equation 4.15, and k' is the factor relating charge density and exposure (equation 4.29).

Thus increasing the voltage applied during charge—up increases the maximum surface charge density which increases the exposure range of the dosimeter. This voltage cannot be increased ad infinitum but is limited by the voltage or surface charge density at which gas multiplication conditions set in (equation 4.16) and also the dielectric strength of the material (e.g. for Mylar, above a potential of 1000 V, the linearity between  $\sigma$  and V is lost 1).

A plot of the saturation current density vs. time (Fig. 4.8) for the same dosimeter configuration as for Fig. 4.2 except for the doubling of the applied voltage during charge—up shows the increased amount of time, and hence exposure, needed to charge and discharge the electret. The charge—up current density reached zero after 120 sec and 240 sec for applied voltages of 40 V and 80 V respectively, with the same times applying from the start of the discharge process. A doubling of the voltage during charging resulted in a doubling of the exposure range of the dosimeter.

A series of charge/discharge curves was acquired for a dosimeter with an air-gap of 2 mm, a collecting electrode radius of 19 mm, a 110  $\mu$ m Mylar electret, and an exposure rate of 0.11 R s<sup>-1</sup>, with the applied voltage ranging from 40 to

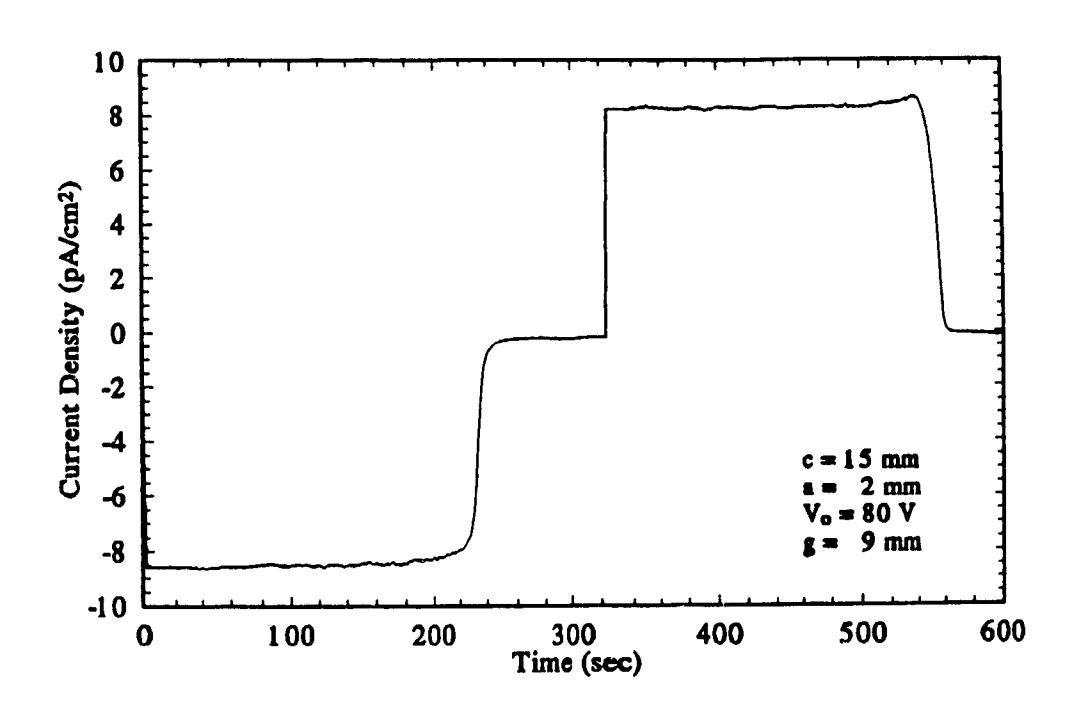


Figure 4.8 A charge/discharge curve of current density versus time for the same dosimeter as Figure 4.2 except for the increase of the initial charging voltage.

1000 V. The discharge curves are shown in Fig. 4.9(a) plotted as the charge removed per unit area collector versus exposure.

į

The discharge curve for a charge—up voltage of 40 V is linear with exposure up to an exposure of about 16 R. At this point there is still a small amount of charge remaining on the electret which is not enough to produce saturation conditions. After this small amount of charge is removed, all the charge deposited on the electret has been depleted so that any further exposure will not increase the total amount of charge removed from the electret. The discharge curve for a charge—up voltage of 80 V follows that of the 40 V exactly but extends to a larger exposure due to the larger initial surface charge density. The same occurs for voltages up to 1000 V where the maximum exposure before loss of linearity is approximately 280 R. A plot of this maximum exposure before loss of linearity occurs is shown in Fig. 4.10.

The upper limit of the exposure range of the dosimeter is determined by three parameters  $-V_o$ , a, and p. The first is the voltage  $V_o$  to which the electret is originally charged, as discussed. The second parameter is the size of the air—gap. A larger air—gap (which would affect k) results in more charge being depleted per incident exposure so that a smaller exposure is needed to deplete the charge layer.

A set of discharge curves for air—gaps ranging from 2 to 8.5 mm is shown in Fig. 4.9(b) with a plot of the charge removed per unit area of the collecting electrode versus exposure. The increased amount of charge removed per unit exposure is seen in the increased slope for increasing air—gaps. The trade—off between sensitivity and the upper limit to the exposure range is evident.

The third parameter affecting the upper limit of the exposure range is the thickness of the electret, p (which would affect  $\lambda$ ). As noted in equation 4.35, a thinner electret results in a larger surface charge density per volt on the electret which again necessitates a larger exposure to totally deplete the charge layer.

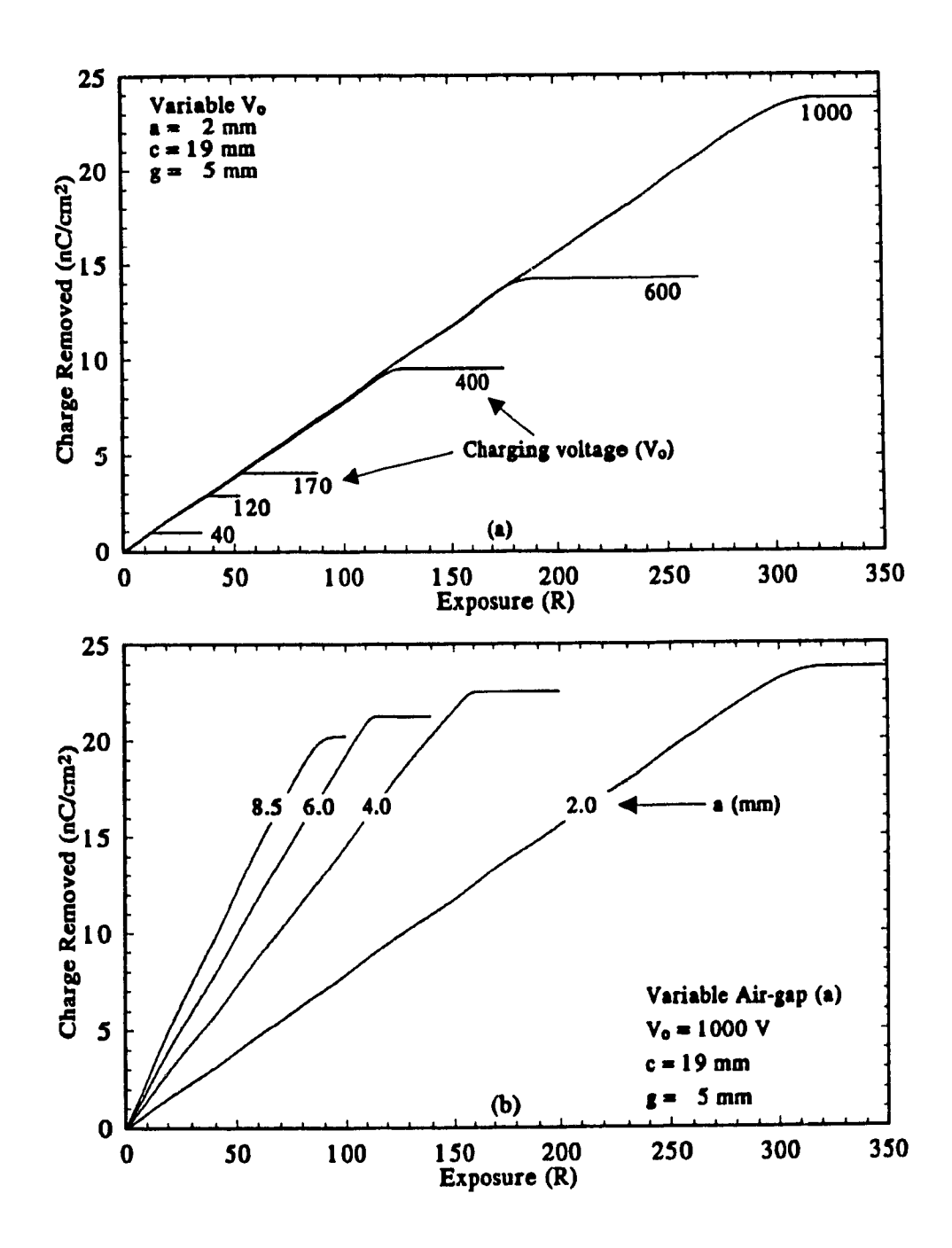


Figure 4.9 Discharge curves of charge density removed versus exposure for (a) constant air-gap and various initial charging voltages and (b) constant voltage and various air-gaps for a 110  $\mu$ m Mylar electret at 90 kVp (effective energy 26 keV), 0.11 R s<sup>-1</sup>.

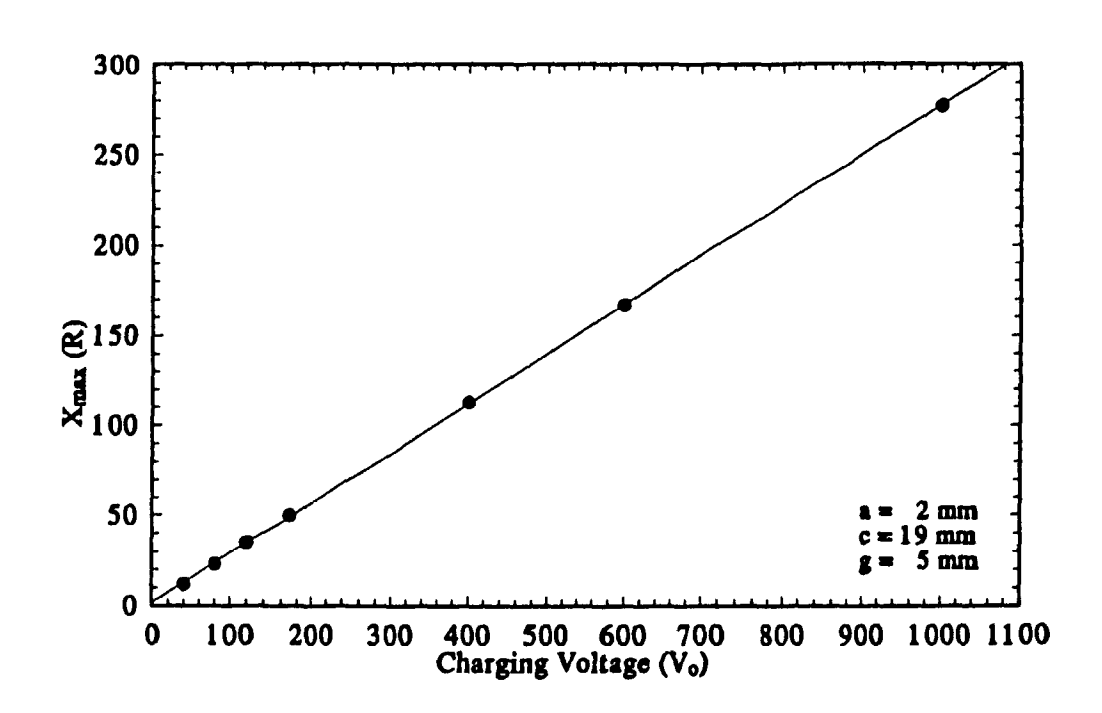


Figure 4.10 Maximum exposure before loss of saturation conditions as a function of charging voltage for a 110  $\mu$ m Mylar electret from the data in Fig. 4.9(a).

The effect of this last parameter, the thickness of the electret, on the surface charge density and hence the upper limit to the exposure range is explained in the following example. An electret which is one tenth the thickness of another electret will reach ten times the surface charge density of the other when both charged to the same voltage. The reason for this can be seen by examining equation 4.2. Keeping  $V_o$ , a, and  $E_a$  constant,

$$pE_p = K (4.39)$$

where  $K=-(V_o+aE_a)$ . Decreasing p requires the increase of  $E_p$  which amounts to an increase in  $\sigma$  since the electric field  $E_p$  is created by the surface charge on the electret.

The effect of p and  $\epsilon_p$  (the dielectric constant of the material) is seen in the following experiment. A dosimeter with a 110  $\mu$ m thick Mylar electret and an air—gap of 4 mm was charged to 80 V. Upon discharging, a total charge of 22.8 nC was removed from the collecting electrode. Another dosimeter with a 25  $\mu$ m thick Teflon electret and the same air—gap was charged to the same voltage. A charge of 58.2 nC was removed from the collecting electrode during discharging. From equation 4.35, the charge density per volt for the Mylar electret,  $\lambda_{\rm myl}$ , is 0.026 nC cm<sup>-2</sup> V<sup>-1</sup> with  $\epsilon_p$  for Mylar equal to 3.2. For the Teflon electret,  $\lambda_{\rm tef} = 0.075$  nC cm<sup>-2</sup> V<sup>-1</sup>, with  $\epsilon_p$  for Teflon equal to 2.1. The ratio of the charge on the Teflon electret and the Mylar electret should be  $\lambda_{\rm tef}/\lambda_{\rm myl} = 2.9$ . Experimentally, it was found to be 58.2 nC/22.8 nC = 2.6. The difference between theoretical and experimental values is due to the unequal areas of the collectors in the two electrets and possible discrepancies in the measurement of the thicknesses of the electrets.

## 4.5.2 Minimum Exposure

The lower limit of the useful exposure range — the minimum detectable exposure — for the electret dosimeter is determined by the accuracy to which the loss of surface charge of the electret due to irradiation is known. To determine this value, the surface charge after exposure is subtracted from the surface charge before exposure. Therefore, inaccuracies may result in the determination of both these values such that the error in the measurement of the charge lost due to irradiation  $\delta_q$  is given by,

$$\delta_q = \sqrt{\delta_i^2 + \delta_f^2} \tag{4.40}$$

where  $\delta_i$  and  $\delta_f$  are the errors involved in the determination of the initial and final charge states, respectively. The minimum detectable exposure is then,

$$X_{min} = \delta_q/k \tag{4.41}$$

where k is the calibration factor for the electret dosimeter.

The determination of the minimum detectable exposure is complicated by two factors — a small leakage current due to the application of the external voltage during charge—up, and a natural decay in the surface charge. These two factors cause the measurement of the charge deposited on the electret during the charge—up process to be consistently greater than the charge measured during the discharge process with no irradiation occurring between the two processes.

The solution to the first problem is simplified by the fact that any current due to the finite resistance of the material between the external voltage and the collecting electrode does not result in the deposition of any charge on the electret surface. During the discharge process, both electrodes are grounded — there is no

external voltage. Therefore, the charge deposited on the electret can be determined by measuring it as it is being removed. Any current measured is due to solely to charge removed from the electret.

An experiment was performed in which an electret with a 2 mm air-gap was charged up to 40 V and immediately discharged with the charge removed from the electret being measured. This process was repeated eight times. Table 4.1 shows the total charge removed for each discharge. The standard deviation  $\delta_i$  for the eight values is 0.008 nC. This would correspond to the fluctuation on the initial deposited charge. The error involved in determining the final charge on the electret is negligible compared to the error on the initial charge. The average standard deviation  $\delta_f$  for a single measurement is  $6.5 \times 10^{-5}$  nC, determined experimentally. For a dosimeter with a calibration factor of 1.5 nC/R and an error in the charge measurement of 0.008 nC, the minimum detectable exposure would be 5 mR.

The exposure range for a given dosimeter configuration can now be summarized. For a 3.8 cm diameter collector, a 110  $\mu$ m thick Mylar electret, an estimate of the error in charge measurement of 0.01 nC, and a maximum charging voltage of 1000 V, the exposure range limits are from low mR to hundreds of R, depending on the air—gap used, as summarized in Table 4.2 (neglecting the effect of various nonlinearities to be discussed further in Chapter 5).

#### 4.6 NATURAL SURFACE CHARGE DECAY MECHANISMS

#### 4.6.1 Introduction

In the development of the formalism describing the operation of the electret dosimeter, the effect of the natural decay of the surface charge has so far been neglected. Of course this cannot be neglected for large errors would result in attributing a loss of charge solely to an exposure when some or all of this loss is due to surface charge decay of the unirradiated electret. The stability of unirradiated

Curve #	Charge (nC)	$\sigma (\text{nC} \times 10^{-5})$
1	4.731	10.33
2	4.735	3.69
3	4.715	8.25
4	4.734	3.89
5	4.722	10.23
6	4.736	5.11
7	4.738	9.07
8	4.747	3.98
Mean	4.727	
$\sigma_{m{n}}$	0.008	
$ar{\sigma}$		6.5

Table 4.1 The charge removed and the standard deviation of each single measurement for a dosimeter with a 110 μm Mylar electret, a 2 mm air—gap, a 12.5 mm radius collecting electrode, and a charging voltage of -40 V repeated 8 times with the mean charge removed and the standard deviation of the 8 values from the mean and the average standard deviation of each single measurement.

EXPOSURE RANGE				
Air—Gap (mm)	Range (R)			
	Min	Max		
1.0	0.020	600		
2.0	0.010	300		
4.0	0.006	150		
6.0	0.004	100		
8.5	0.003	80		

Table 4.2 Exposure range for an electret dosimeter with a 110  $\mu m$  Mylar electret, a 19 mm collector radius, an estimate of the minimum detectable charge difference of 0.01 nC, and a maximum charging voltage of 1000 V.

electrets depends on a variety of factors including temperature, humidity, electret material, and the method of formation of the electret. Due to its superior charge Temperature retention characterisics, Teflon is the electret material of choice. variations within the range normally encountered in regular daily living will not affect the stability of charge on the Teflon electret since temperatures of 150° C to 200° C are required to release charges found in the deep traps in which the stable charges are found (from thermally stimulated current release studies<sup>14</sup>). excellent charge retention capabilities of Teflon under high humidity conditions has been attributed to the hydrophobic behavior of this material 15. MacDonald<sup>16</sup> performed charge retention studies on electrets charged with the method used here and found that after an initial stabilization period of about 10 days in which the potential above the electret surface dropped to 75-85 % of the initial value (depending on electret material and other factors), the rate of decay slowed to 0.04 % of the initial charge per day for Teflon. The two mechanisms responsible for this decay are radiation-induced conductivity and trap-modulated mobility.

# 4.6.2 Radiation-Induced Conductivity

1

N

Normally most dielectrics have a very low conductivity. It is this feature which allows them to exhibit excellent charge retention capabilities. Exposing a dielectric to ionizing radiation increases its conductivity. This is a natural phenomenon due to the lifting of free electrons into the conduction band and free holes into the valence band by the ionizing radiation. This radiation—induced conductivity (RIC) is dose rate dependent as can be seen from the relation  $^{17}$  between the steady—state RIC, g, and the dose rate,  $\dot{D}$ ,

$$g = g_0(\dot{D}/\dot{D}_0)^{h}, \quad 0.5 < \Delta < 1$$
 (4.42)

where  $\dot{D}_o$  is a reference value taken as 1 rad/s and  $g_o$  the conductivity at that value. The radiation—induced current density  $j_{rad}$  across the polymer is,

$$j_{rad} = gE (4.43)$$

where E is the electric field across the thickness of the polymer.

Immediately after the cessation of the irradiation, the conductivity is reduced to a fraction  $\theta$  of its steady state value, followed by a continuous drop in the conductivity 18 according to,

$$g(t) = \theta g(1 + t/\tau^*)^{-1} \tag{4.44}$$

where  $\tau^*$  is a time constant which depends on g(0) and is typically smaller than 1 min. The delayed radiation—induced current density  $j_{del}$  across the polymer is,

$$j_{do}(t) = g(t)E(t) \tag{4.45}$$

where E(t) is the time-dependent electric field across the thickness of the polymer. Thus there is a delayed radiation-induced conductivity (DRIC) component giving rise to a delayed radiation-induced current which continues for a very long time after the termination of the irradiation. This phenomenon is partially responsible for the observed decay of the surface charge after the charging of the dosimeter. Values for Teflon<sup>19</sup> are  $\Delta = 0.7$ ,  $g_o = 1.7 \times 10^{-16} \ \Omega^{-1} \ \mathrm{cm}^{-1}$ ,  $\theta = 1/3$ , and  $\tau^* = 1 \ \mathrm{s}$ . For a dose rate of 0.11 rad s<sup>-1</sup>, typical for the radiation source used, the radiation-induced conductivity is  $g = 3.6 \times 10^{-17} \ \Omega^{-1} \ \mathrm{cm}^{-1}$ . With a voltage at the electret surface of 1000 V across 25  $\mu \mathrm{m}$  of Teflon,  $j_{rad} = 14.4 \ \mathrm{pA} \ \mathrm{cm}^{-2}$ . This would quickly drop to one third of this value at the termination of the irradiation -  $j_{del}(0) = 4.8 \ \mathrm{pA} \ \mathrm{cm}^{-2}$  and would subsequently decay according to equation 4.44.

This surface charge decay phenomenon can explain the relatively large standard deviation of the repeated charge/discharge process discussed in the section 4.5.2.. Small variations in the time between charging and discharging lead to variations in the amount of charge removed during the discharge process.

The decay of the surface charge density of an unirradiated electret can be observed by measuring the current passing through the electrometer to ground, without irradiation. A dosimeter was charged up to 1000 V after which the irradiation was halted and the external voltage removed. A current of 15 pA was measured and determined to be due to the natural decay of the surface charge. This current was observed to decay to 0.5 pA after 21 hours (see Fig. 4.11).

This RIC and DRIC could complicate the determination of exposure to the dosimeter in a high dose rate situation since there would be a reduction in the charge on the electret due to the collection of ions and an additional reduction due to the induced conductivity. However at lower dose rates, as those normally encountered in personnel dose monitoring, the small increase in conductivity due to irradiation has a minimal effect on the signal.

# 4.6.3 Trap-Modulated Mobility

1

T.

Another effect responsible for surface charge decay in an electret is the inherent mobility of charges in an electric field. The free mobility  $\mu_0$  is the mobility of electrons in the conduction band or holes in the valence band and is given by,

$$v = \mu_o E \tag{4.46}$$

where v is the velocity of charges with a free mobility  $\mu_o$  in an electric field E. A typical value<sup>20</sup> is 10 cm<sup>2</sup> V<sup>-1</sup> s<sup>-1</sup>. The trap—modulated mobility  $\mu$  is the

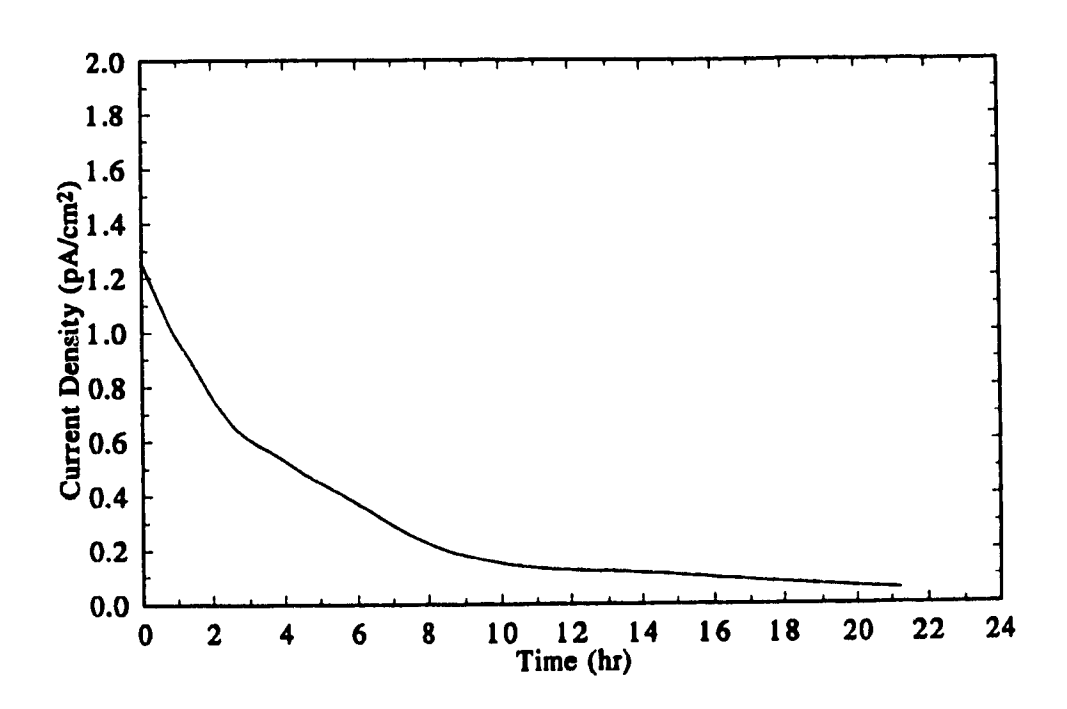


Figure 4.11 Current density for c=19 mm as a function of time after the charging of a dosimeter illustrating the current measured due to the decay of surface charge of the unirradiated electret and the decrease in the rate at which this charge is decaying (110  $\mu$ m Mylar electret initially charged to 1000 V).

mobility of charges in the presence of traps. Deeper energy traps result in a decreased value for  $\mu$  while shallow energy traps result in a value for  $\mu$  closer to the free mobility,  $\mu_o$ . The current density due to charge mobility is,

1

A.

$$j_{moh} = \mu \rho E \tag{4.47}$$

where  $\rho$  is the sum of the free and trapped charge densities. In the presence of shallow traps, the mobility  $^{20}$  is  $10^{-3}$  cm $^2$  V $^{-1}$  s $^{-1}$ . The steady-state (i.e. deep traps) trap modulated mobility for electrons in Teflon $^{21}$  is  $10^{-17}$  cm $^2$  V $^{-1}$  s $^{-1}$ . This gives a current density due to the mobility of the charges for a typical charge density of 25 nC cm $^{-3}$  and a potential of 1000 V across a 25  $\mu$ m thick polymer of,  $j_{mob} = 10^{-19}$  C cm $^{-2}$  s $^{-1}$ . This value holds for steady-state conditions. The presence of many shallow traps causes this value to be time-dependent with an initial value much greater than the value quoted due to the large trap-modulated mobility of charges found in shallow traps. The number of deep volume traps is limited to about  $1.4 \times 10^{14}$  cm $^{-3}$ , therefore a 25  $\mu$ m thick Teflon film can store only a projected charge density of 28 nC cm $^{-2}$  – equivalent to a surface voltage of 376 V – for long periods of time $^{22}$ .

The steady—state trap modulated mobility for holes in Teflon<sup>21</sup> is 10<sup>-9</sup> cm<sup>2</sup> V<sup>-1</sup> s<sup>-1</sup>, many orders of magnitude greater than that of electrons in Teflon. Thus, for increased charge stability, Teflon electrets are always charged with negative charge carriers.

### 4.6.4 Modification of Formalism

The formalism developed earlier in the chapter to describe the relation between the surface charge density and the exposure must now be modified to account for the decay of the unirradiated electret. Incorporating equations 4.20 and 4.28,

$$\sigma(X) = \sigma_r - X[\kappa a + \lambda' \nu \{1 - \exp(3a/a_r)\}]$$
 (4.48)

where  $\sigma_r$  the remaining surface charge density, is given by,

$$\sigma_r = \sigma'(1 - c_0 t) \text{ for } t_d < t < 1/c_0$$
 (4.49)

$$\sigma' = \psi \sigma_0 \tag{4.50}$$

 $\psi$  is obtained by extrapolating the linear portion of the  $\sigma$  versus t plot to t=0.  $t_d$  is the stabilization period after which the linear surface charge decay ensues. Equation 4.48 takes into account the surface charge decay of the unirradiated electret, the decay of charge due to the collection of ions created by the direct interaction of photons with air, and the decay of charge due to the collection of ions created by the photoelectrons emitted from the material surrounding the sensitive volume. Thus the charge lost due to decay, known a prior for a given time, is subtracted from the charge lost due to the ionization of the air.

The maximum exposure which can be measured with the dosimeter involves the modification of equation 4.38:

$$X_{max} = \frac{\sigma_r(t=T) - \sigma_{sat}}{k'} \tag{4.51}$$

where

$$\sigma_r(t=T) = \sigma'(1-c_oT) \tag{4.52}$$

and T is the total time the dosimeter is in the field.

The minimum exposure is still given by equation 4.41, but the error in charge measurement must now allow for errors due to natural charge decay,

$$\delta_q = \sqrt{\delta_{\sigma'}^2 + \delta_f^2 + \delta_{decay}^2 T^2}$$
 (4.53)

where  $\delta_{\sigma'}$  is related to the error in the determination of the level to which the charge density decays before the linear decay ensues,  $\delta_f$  is the error in determining the final charge state,  $\delta_{decay}$  is the error in determination of the rate of natural decay, and T is the total time the dosimeter is the field. Studies are being continued to determine the magnitude of these parameters.

### 4.7 PREPARATION OF TEFLON ELECTRETS

4

A discharge curve for a dosimeter with a fresh, virgin Teflon electret is shown in Fig. 4.12(a). The saturation current density began at a constant value, as predicted by theory, however, instead of dropping quickly to zero, the current density decayed to twenty percent of its saturation value and then decayed at a much slower rate to zero current density. This "tail" to the discharge curve has serious implications. The task of determining the charge remaining on the electret is much more difficult since the dosimeter must be irradiated for very long periods of time — in this case, thousands of seconds instead of two hundred seconds if the discharge dropped quickly to zero.

To attempt to determine the origin of this discharge—tail, a study was undertaken in which the dosimeter was charged for a fixed time, 130 seconds, at a range of voltages after which it was immediately discharged to determine the effect on the tail. In Fig. 4.12(b), the end of the discharge curve is shown for each of the

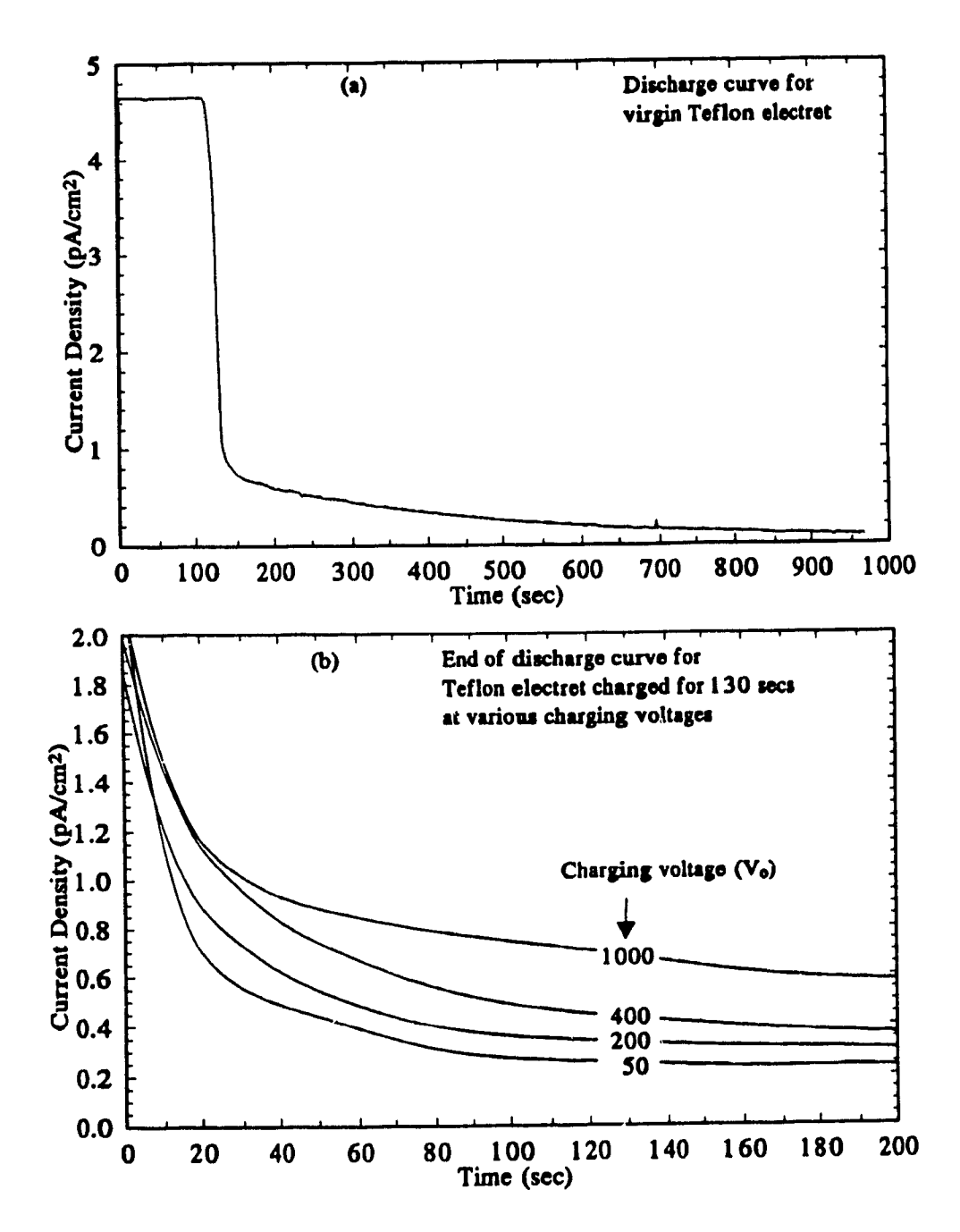


Figure 4.12 (a) A discharge curve for a virgin 75  $\mu$ m Teflon electret (c=19 mm, a=2 mm,  $V_o=-50$  V, 0.11 R s<sup>-1</sup>) showing the anomalous "tail" at the end of the discharge; (b) a plot of current versus time for the end of the discharge curve showing the effect of increasing the charge—up voltage on the tail.

charging voltages tested. The level to which the post—saturation current density decayed increased with increasing charging voltage. Thereafter, the current density decreased at approximately the same rate. It was postulated that a volume—charge effect was responsible for this anomaly. Under irradiation, charge carriers are created in the polymer as well as in the air above it. With the application of an electric field, these charge carriers get separated leading to the space—charge polarization of the electret (as in the radioelectret discussed in section 2.3.2). The increased voltage during charging augmented this effect, possibly leading to the increased space—charge polarization responsible for the observed tail.

Another experiment showed that heating the virgin Teflon eliminated the tail. The end of a discharge curve for a virgin Teflon electret is shown in Fig. 4 13 (unheated). The electret was then heated to a temperature of 250°C at a rate of 3°C per minute and quickly cooled to room temperature by immersing the electret in water. It was then charged and discharged. The end of the discharge curve is again shown in Fig. 4.13 (heated). It is seen that the current density now decayed quickly to zero as compared to the curve for the unheated Teflon. Simply heating the Teflon eliminated the tail. Possibly the heating process altered the distribution of charge—traps in the bulk of the Teflon resulting in a loss of traps necessary to form the space—charge polarization.

Į.

4

### 4.8 DIFFERENCES BETWEEN VOLTAGE AND CHARGE READ-OUT

Electret dosimeters depending on the measurement of the voltage at the electret's surface differ from the proposed electret dosimeter in one important aspect: the thickness of the electret affects the sensitivity of the dosimeter as well as the range, whereas when measuring charge densities, the thickness of the electret only influences the range of the dosimeter and not the sensitivity. Consider the differential form of equation 4.5,

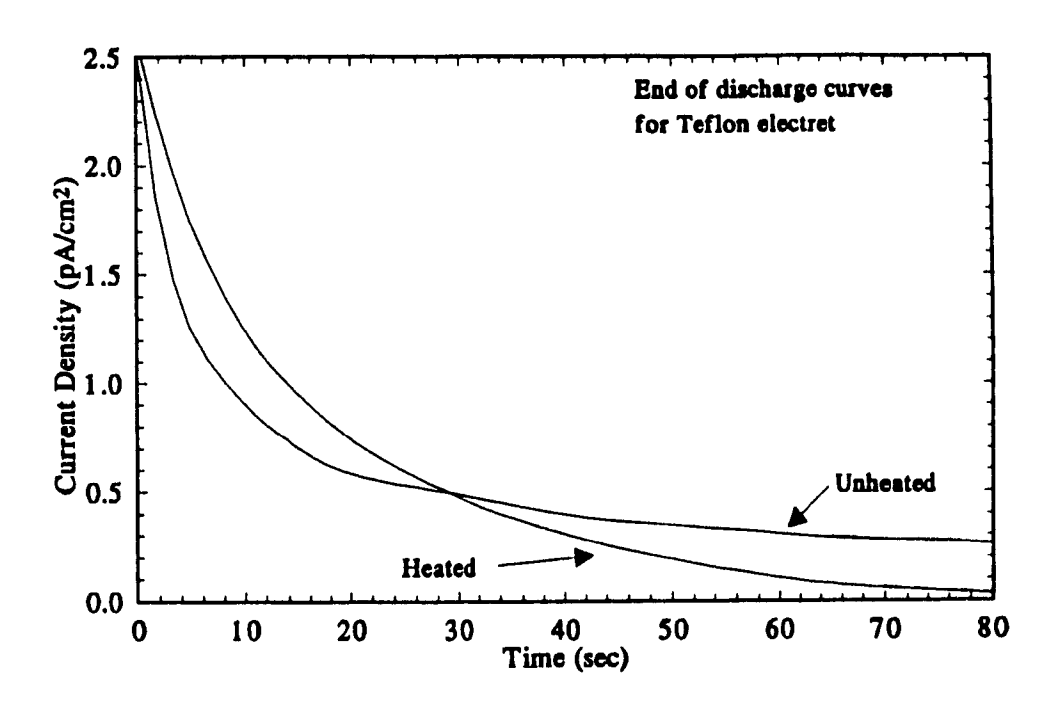


Figure 4.13 A plot of current versus time for the end of the discharge curve of a virgin Teflon electret showing the elimination of the "tail" by heating the electret to 250° C and quickly cooling the electret to room temperature before charging.

$$\Delta V = -\Delta \sigma p / \epsilon_0 \epsilon_p \tag{4.54}$$

With the sensitivity defined as the change in voltage for a given exposure,

$$\Delta V/\Delta X = -\Delta \sigma p/\Delta X \epsilon_o \epsilon_p \tag{4.55}$$

Substituting equation 4.20,

$$\Delta V/\Delta X = -\kappa a p/\epsilon_o \epsilon_p \tag{4.56}$$

It is evident from equation 4.56 that an increase in parameter p, the thickness of the electret, will increase the sensitivity as will an increase in the air—gap whereas, by examining equation 4.20, the thickness of the electret has no effect on the sensitivity when measuring the surface charge.

Another important difference between the two methods is the fact that the variation of the area of the collecting electrode has no effect on the sensitivity in the voltage mode since the change in voltage above the electret surface has no dependence on the area of the electret. When measuring charge, the variation of the area of the collecting electrode is effectively changing the sensitive volume from which charge carriers are collected and measured thus the sensitivity is strongly dependent on the area of the collecting electrode.

## REFERENCES

- <sup>1</sup>B. G. Fallone and E. B. Podgorsak, "Production of Foil Electrets by Ionizing Radiation in Air", Phys. Rev. B 27, 2615-2618 (1983).
- 2G. M. Sessler, "Electric Fields and Forces due to Charged Dielectrics", J. Appl. Phys., 43, 405-408, (1972).
- <sup>3</sup>B. G. Fallone and E. B. Podgorsak, "Dynamics of radiation—induced charging and discharging of foil electrets", Phys. Rev. B 27, 5062-5065 (1983).
- 4B. G. Fallone and E. B. Podgorsak, "Saturation curves of parallel-plate ionization chambers", Med. Phys. 10, 191-196 (1983).
- <sup>5</sup>G. Mie, "Der Elektrische Strom in Ionisierter Luft in Einem Ebenem Kondensator", Ann. Phys. 13, 857-889 (1904).
- 6H. Seeman, "Messung der Sättigungsstromkurve in Luft, die mit Röntgenstrahlen ionisiert ist", Ann. Phys. 38, 781-785 (1912).
- 7F. H. Attix, Introduction to Radiological Physics and Radiation Dosimetry, (John Wiley and Sons, New York, 1986), p.439.
- 8M. Ikeya, K. Mahesh and D. R. Vij (Eds.). Techniques of Radiation Dosimetry, (John Wiley & Sons, New York, 1985), p. 257.
- <sup>9</sup>Ibid., p. 256.
- <sup>10</sup>B. G. Fallone and J. A. Bencomo, "A linear-quadratic fit for saturation curves obtained under continuous irradiation of parallel-plate ionization chambers", Med. Phys. 14, 359-364 (1987).
- <sup>11</sup>B. G. Fallone and E. B. Podgorsak, "Radiation-induced foil electret chamber", Phys. Rev. B 28, 4753-4760 (1983).

<sup>12</sup>H. E. Johns, J. R. Cunningham, *The Physics of Radiology*, (Charles C Thomas, Springfield, Illinois, 1983), p.234.

<sup>13</sup>Ibid., p.149.

14G. M. Sessler, Topics in Applied Physics Vol.33: Electrets, 2nd ed. (Springer-Verlag, New York, 1987), p.57.

<sup>15</sup>Ibid., p.69.

16B. MacDonald, "Surface Charge Characteristics of the Radio-charged Electret", M.Sc. thesis, McGill University, 1990.

<sup>17</sup>B. Gross, G. M. Sessler (Ed.), *Topics in Applied Physics Vol.33: Electrets*, 2nd ed. (Springer-Verlag, New York, 1987), p.219.

18G. M. Sessler, Topics in Applied Physics Vol.33: Electrets, 2nd ed. (Springer-Verlag, New York, 1987), p.220.

19B. Gross, G. M. Sessler (Ed.), Topics in Applied Physics Vol.33: Electrets, 2nd ed. (Springer-Verlag, New York, 1987), p.243.

<sup>20</sup>G. M. Sessler, Topics in Applied Physics Vol.33: Electrets, 2nd ed. (Springer-Verlag, New York, 1987), p.72.

<sup>21</sup>Ibid., p.73.

\*

<sup>22</sup>G. M. Sessler, D. A. Seanor (Ed.), *Electrical Properties of Polymers*, (Academic Press, New York, 1982), p.269.

### CHAPTER 5

### ELECTRODE EDGE EFFECTS

### 5.1 INTRODUCTION

The study of edge-effects in parallel plate ion chambers has been scarce. Most theoretical analyses of parallel plate arrangements assume infinite area electrodes or casually mention the possibility of discrepancies due to edge effects. These edge effects are variations in the direction and strength of the electric field near the edge of parallel-plate electrodes due to the absence of electrode material beyond the edge of the electrode. To minimize these effects, a guard-ring is used. The guard-ring is a ring of electrode material which surrounds the collecting electrode but is electrically distinct from it, the signal from which is not measured but is shunted directly to ground. The purpose of the ring is to define the volume from which ions are collected by relegating the fringe-field region at the edge of the electrodes to the guard-ring so that the electric field lines over the collecting electrode remain uniform and perpendicular to the surface of the electrode. Guard-rings are used in parallel plate ionization chambers, however their purpose is primarily to prevent leakage current from the polarizing electrode from being measured. Indeed, the theoretical development leading to the description of the electret dosimeter charge/discharge curve assumes that the electric field lines across the entire electret covering the collecting electrode are uniform and parallel - edge effects were neglected.

These edge effects cannot, in fact, be neglected for they have a profound effect on the response of the electret dosimeter to irradiation. Ideally, the guard ring would extend to infinity, however the requirement that the dosimeter be

physically compact restricts the width of this ring. This restriction leads to the eventual collection of ions from the fringe-field region, the size of which increases as the electret surface charge density decreases due to irradiation.

#### 5.2 VARIATION OF THE GUARD-RING WIDTH

## 5.2.1 The guard—ring study

-

The discharge curve of charge vs exposure for an air—gap of 8.5 mm (Fig. 4.9) seems to be agree well with the theory developed using the laws of Gauss and Kirchoff developed in section 4.2. The sensitivity is greater than configurations with smaller air—gaps, seen in the greater slope as compared to the curves with the smaller air—gaps, and the charge vs. exposure curve is linear up to the point where the surface charge has been fully depleted. Closer examination of the charge vs. exposure curve for the 8.5 mm air—gap reveals that this last statement is, in fact, not true. The slope of the curve gradually decreases at higher exposures as can be seen in Fig. 5.1(a) where the same curve is plotted with a straight line of slope equal to the initial slope of the curve fitted to the data. This phenomenon is easier to visualize with the corresponding current vs. time curve from which this charge vs. exposure curve was derived (see Fig. 5.1(b)). The theory predicts a constant saturation current followed by a quick drop to zero current. From the graph it is seen that the saturation current is not constant, but is continuously decreasing.

It was postulated that the reason for this continually decreasing saturation current is related to the size of the guard-ring. An experiment was performed to further explore this effect. In this experiment, the radius of the collecting electrode was kept fixed at c = 12.5 mm while the width of the guard-ring was varied for a series of different air-gaps. The radius of the polarizing electrode was varied so that it always equaled the sum of the radius of the collecting

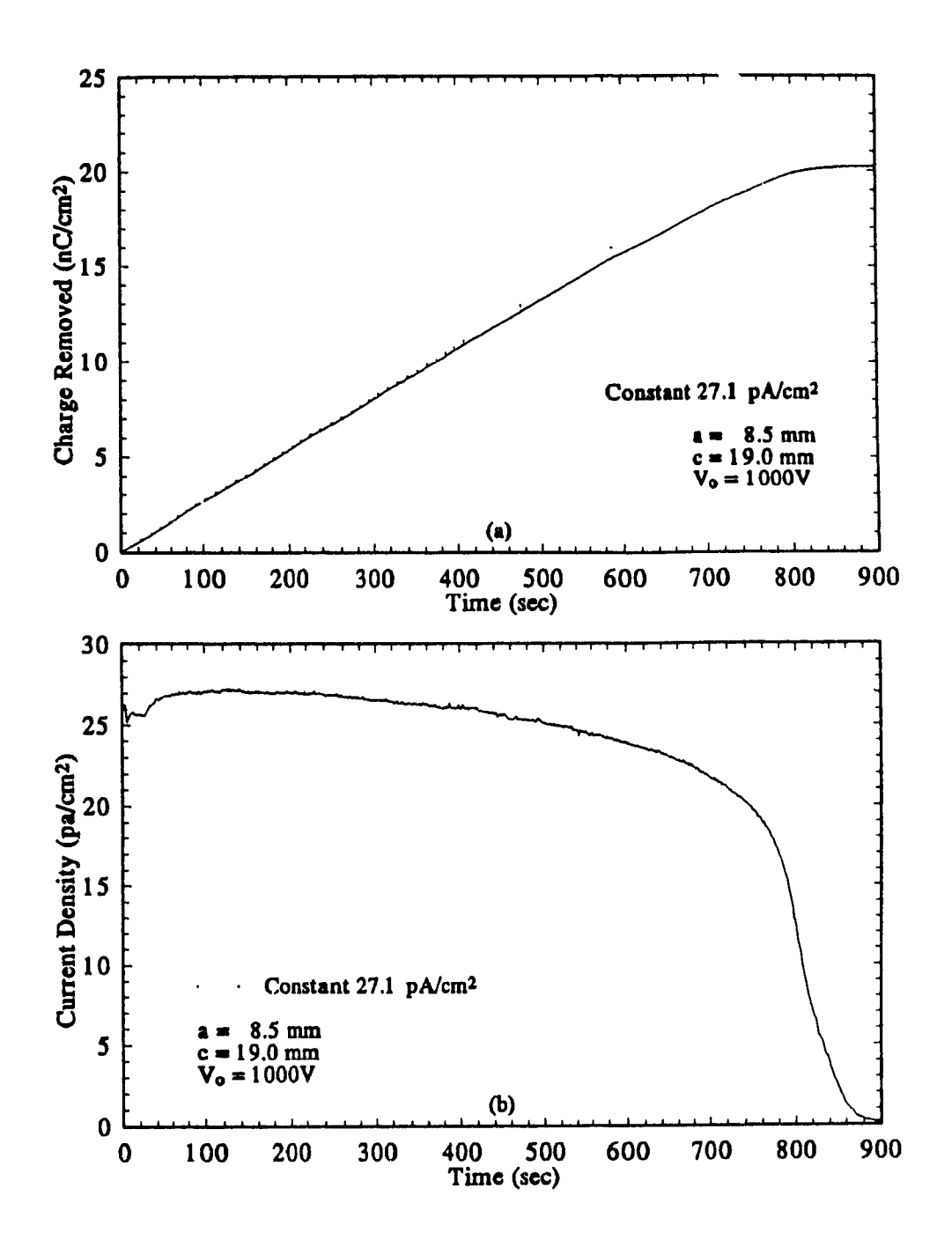


Figure 5.1 (a) The discharge curve of charge removed versus time for a=8.5 mm from Fig. 4.9(b) with a fitted line of slope equal to the initial slope of the curve; (b) the corresponding plot of current density versus time  $-110~\mu\mathrm{m}$  Mylar electret, 0.11 R s<sup>-1</sup>.

electrode and the width of the guard-ring. Thus the diameter of the polarizing electrode and the diameter of the collecting electrode with its guard-ring were always equal. A charge/discharge curve was acquired for each configuration with five values of the guard-width g ranging from 1.0 to 10.0 mm, and five different air-gaps a ranging from 1.5 to 10.0 mm for a total of twenty-five configurations.

Frage 4

1

Fig. 5.2 shows the general trends which were observed. Fig. 5.2(a) shows a set of discharge curves in which the guard ring width was kept constant at g=1.0 mm and the air—gap varied. In this configuration, the radius of the polarizing electrode was 13.5 mm (the sum of g=1.0 mm and c=12.5 mm). With a=1.5 mm, the saturation current is relatively constant until the end of the discharge curve where the current quickly drops to zero. The curve for a=2.6 mm exhibits a continuously declining saturation current with an average slope  $m_{sat}$  over the first 35 seconds of -0.3 pA/sec. As a is increased, the slope continues to steepen until at a=10.0 mm,  $m_{sat}=-7.2$  pA/sec.

The reason for this declining saturation current whose rate of decline increases with increasing air—gap is related to the varying size of the fringe—field region at the edge of the electrodes. A guard—ring which is too small results in ions being collected and measured from this fringe—field region, the size of which varies as the surface charge density changes. With a small air—gap of 1.5 mm, the size of this fringe—field region is small enough such that a 1.0 mm guard—ring is sufficient. At larger air—gaps, there is a larger degree of fringing of the electric field lines at the edge of the electrodes — the size of the fringe field region increases — such that the 1.0 mm guard—ring is no longer sufficient.

Fig. 5.2(b) shows a set of discharge curves in which the air-gap was kept constant at a = 10.0 mm and the width of the guard-ring varied. Now the average rate of decline decreases from a value of -6.3 pA/sec for g = 2.5 mm to a value of -0.3 pA/sec for g = 10 mm. Increasing the width of the guard-ring decreased the

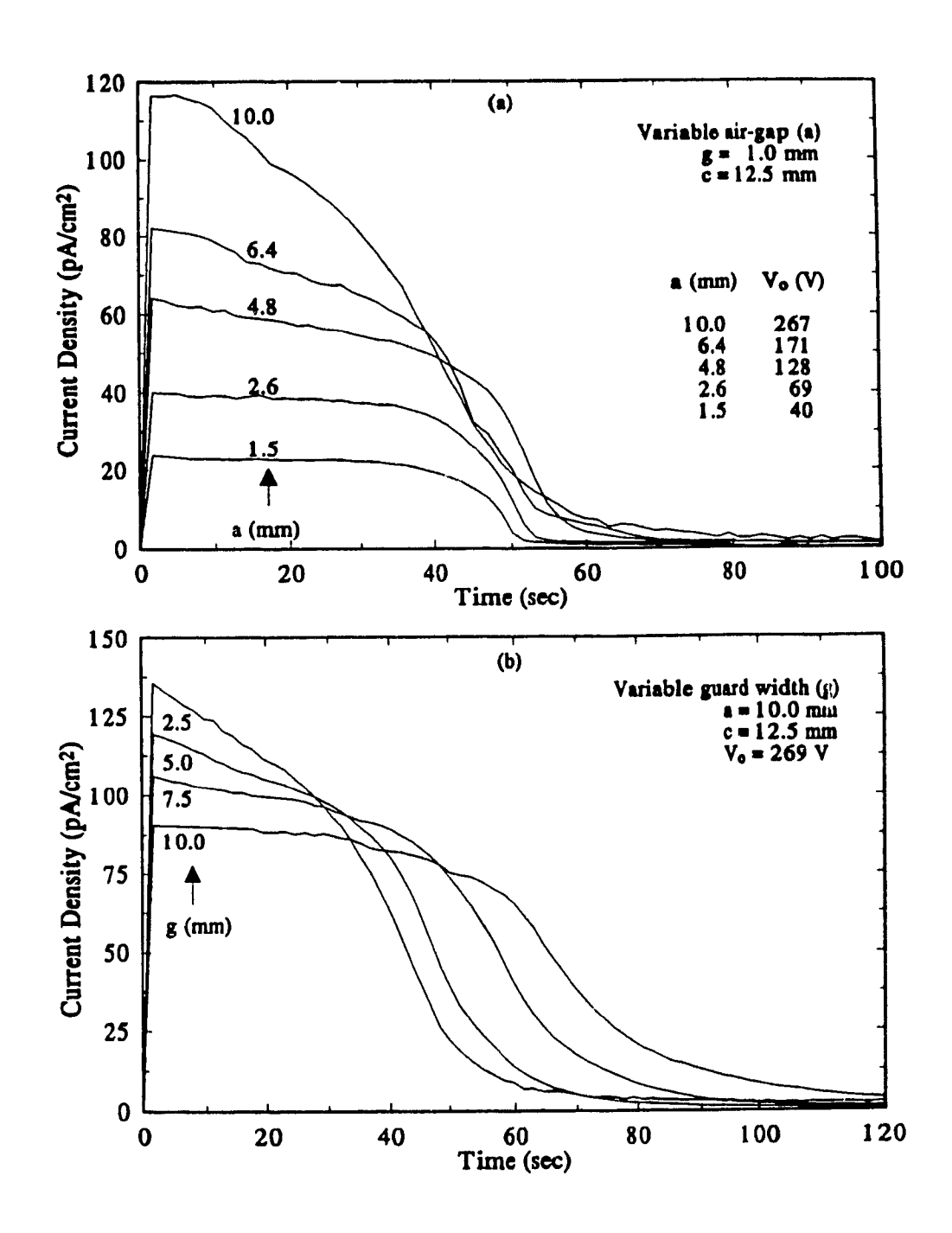


Figure 5.2 A set of discharge curves plotting current density versus time for a 110  $\mu$ m Mylar electret for (a) constant guard-ring width and variable air-gap and (b) constant air-gap and variable guard-ring width at 0.11 R s<sup>-1</sup>.

rate of decline of the saturation current due to the fact that a smaller portion of ions from the fringe—field region were being collected and measured by the collecting electrode. Thus a fairly large guard—ring is needed for this large air—gap.

A plot of the rate of decline of the saturation current  $m_{sat}$  versus the width of the guard-ring g for different air-gaps a is shown in Fig. 5.3. The general trend is for the value of  $|m_{sat}|$  to increase with decreasing g for all a and with increasing a for all g. A guard-ring width of 10 mm was sufficient to bring  $m_{sat}$  close to zero for all the air-gaps tested. For the smaller air-gaps,  $m_{sat}$  did not deviate much from zero in the whole range of guard-ring widths tested.

In an attempt to better quantify the width of guard-ring needed for a given air-gap in order to bring the rate of decline of the saturation current close to zero, the data shown in Fig. 5.3(a) was replotted as  $m_{sat}$  vs.  $\sqrt{g}/a$  (Fig. 5.3(b)). From the graph it is apparent that in order for  $m_{sat}$  to be close to zero, the following relation must hold,

$$\sqrt{g}/a \ge 0.6 \text{ mm}^{-1/2}$$
 (5.1)

for a 12.5 mm radius collecting electrode. Thus for an air-gap of 5 mm, the width of the guard-ring should be  $g = (a \times 0.6)^2 = 9$  mm.

### 5.2.2 Calibration with Nonlinearities

14.

The calibration factor for a specific dosimeter configuration is obtained by determining the ratio of the saturation current and the known exposure rate. If the response of the dosimeter to irradiation is continually changing with exposure – i.e. the saturation current exhibits a continuous decline – it would seem that the

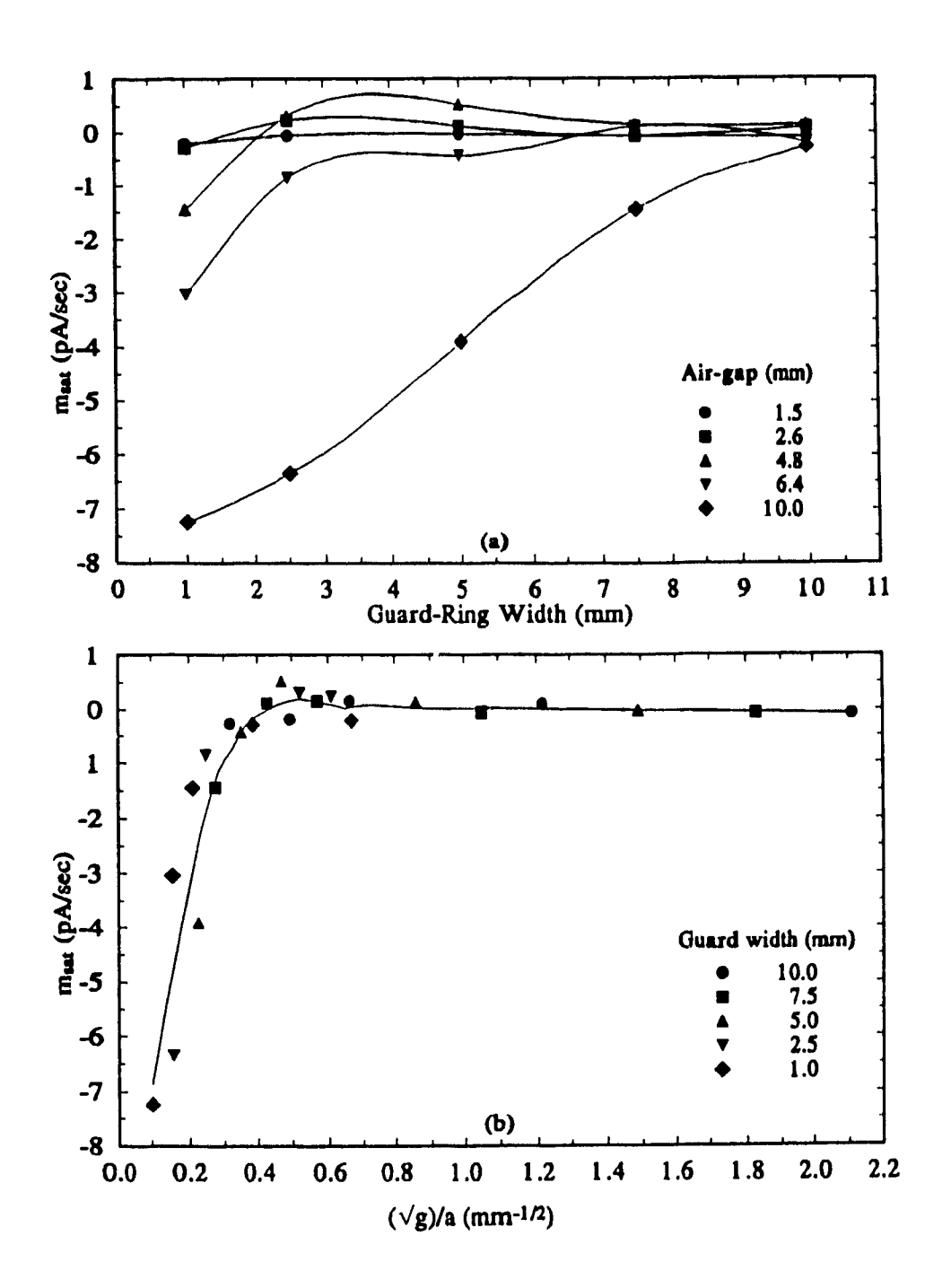


Figure 5.3 (a) The slope  $m_{sat}$  of the initial flat portion of the current profile as a function of guard-ring width for different air-gaps; (b) the same data plotted versus  $(\sqrt{g})/a$ .

calibration factor cannot be determined. The usefulness of the second method of determining the calibration factor is now apparent.

By analyzing the charge vs. exposure curve instead of the current vs. time curve, it is possible to fit a straight line to the data and use the slope of this fitted line as the value for the calibration factor. It is obvious that a certain margin of error will be introduced due to the imperfect fit of the data to the line, however imposing certain limits on the useful exposure range can minimize these errors.

Consider the current curve for a = 10.0 mm, g = 1.0 mm, c = 12.5 mm given in Fig. 5.2(a). The charge vs. exposure curve which results by multiplying the abscissa by the exposure rate and integrating is shown in Fig. 5.4(a). A straight line has been fitted to the data corresponding to the charge curve that would result if the saturation current was constant at its initial value. It seems that the fit is perfect for the first roentgen of exposure. After this, the two curves diverge. Even at 1 R, where the two curves appear to be coincident, the difference between the two curves is 0.06 nC which for a calibration factor here of 5.3 nC/R corresponds to an error of 11 mR with the error increasing with exposure. A straight line with a different slope might fit the data over a larger exposure range. Consider a slope of 4.7 nC/R. The largest error below 3 R, where the two curves cross, is 0.69 nC giving an error of 130 mR.

To and

J

It must be pointed out that this is exactly the methodology used for determining the calibration factor and the exposure range over which this factor applies in all electret dosimeters relying on the measurement of the potential above the electret surface. The charged electret dosimeter is submitted to a series of exposures with the reduced voltage being measured after each exposure. This data is plotted on a graph of voltage vs. exposure and a straight line is fitted over a

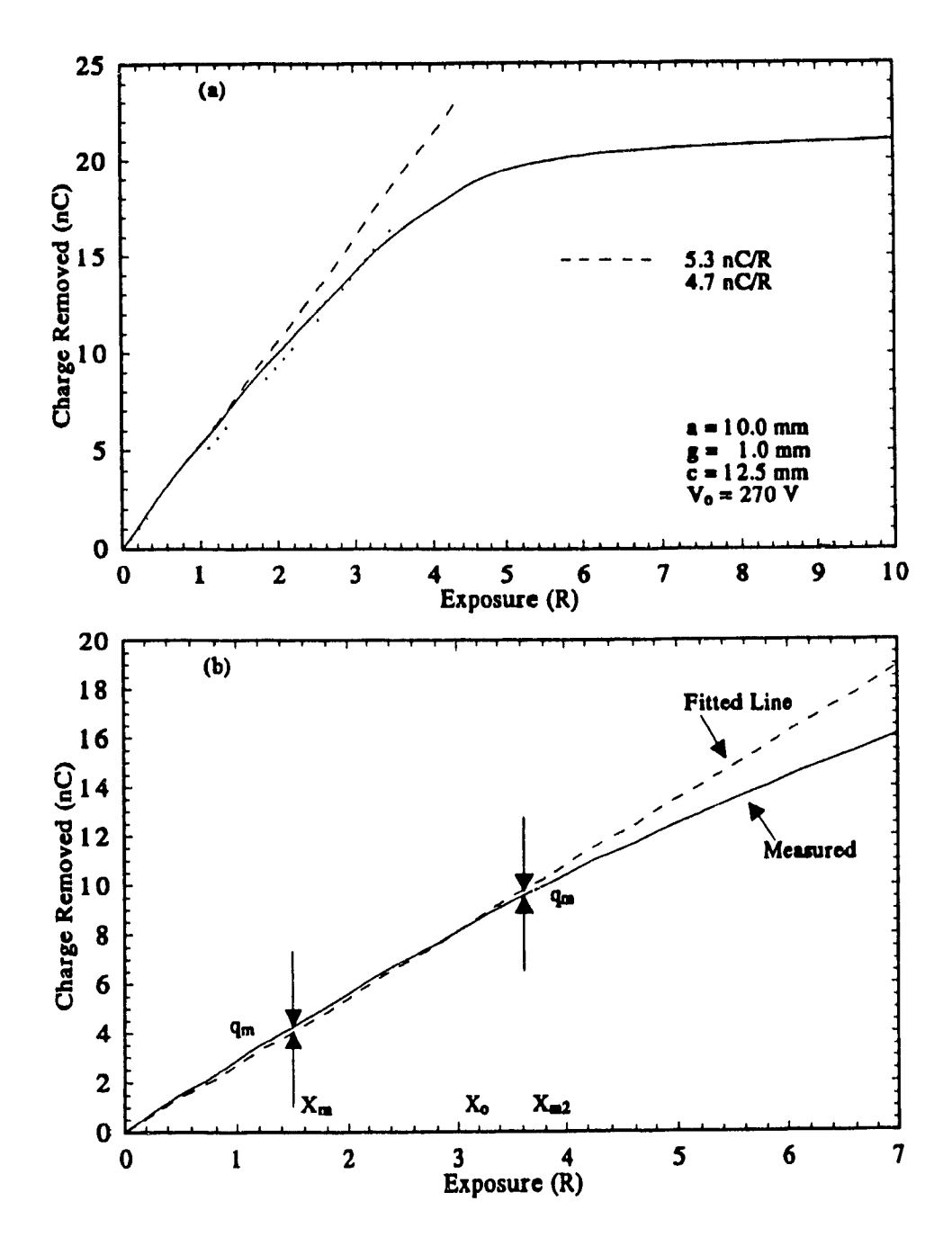


Figure 5.4 (a) Discharge curve of charge removed versus exposure for a 110  $\mu$ m Mylar electret illustrating the loss of linearity as the discharge process continues with two fits to the data; (b) a schematic plot of charge removed versus exposure for a continual change in the saturation current of -2.0 pA/sec with a fit to the data.

portion of this data, the slope of which gives the calibration factor in units of V/R. Small errors introduced by a dosimeter which exhibits a continuous decline in response when exposed are difficult to detect in this method.

A prediction of the errors introduced by this continuous variation in the response of the dosimeter with exposure can be made more quantitative by making one simplifying assumption: a constant slope of the saturation current  $m_{sat}$  is assumed equal to the average slope over the initial portion of the current curve. The current is given by,

$$I(t) = I_o + m_{sat}t (5.2)$$

where  $I_o$  is the initial current, and the charge as a function of time is given by

$$q(t) = \int_0^t (I_0 + m_{sat}t) dt$$
 (5.3)

$$q(t) = I_0 t + m_{sat} t^2 / 2 (5.4)$$

assuming q(0) = 0. With  $t = X/\dot{X}$  and using X as the independent variable,

$$q(X) = I_o X/\dot{X} + m_{sat} (X/\dot{X})^2/2$$
 (5.5)

The straight curve which is fitted to the data is given by,

$$q_{fit}(X) = kX (5.6)$$

The difference  $q_{diff}$  between the fitted straight line and the actual curve is

$$q_{diff}(X) = q_{fit}(X) - q(X)$$
 (5.7)

$$q_{diff}(X) = kX - I_0 X/\dot{X} - m_{sat} (X/\dot{X})^2/2$$
 (5.8)

The exposure  $X_o$  at which the difference between the two curves is zero is found by setting the above expression to zero and solving for X to get,

$$X_{o} = 2\dot{X}^{2}(k - I_{o}/\dot{X})/m_{sat}$$
 (5.9)

The exposure at which the maximum difference between the two curves occurs  $X_m$  is found by differentiating  $q_{diff}(X)$  with respect to X, setting the result equal to zero and solving for X:

$$dq_{diff}/dX = (k - I_o/\dot{X}) - m_{sat}X/\dot{X}^2$$
 (5.10)

$$X_m = (k - I_o/\dot{X})\dot{X}^2/m_{sat} = X_o/2$$
 (5.11)

The actual value of this maximum difference  $q_m$  is found by substituting  $X_m$  into equation 5.8,

$$q_m = (k - I_o/\dot{X})^2 \dot{X}^2 / 2m_{sat}$$
 (5.12)

The upper exposure at which this same difference in charge occurs is at  $X_{m2}$ 

$$X_{m2} = (1 + \sqrt{2})(k - I_o/\dot{X})\dot{X}^2/m_{sat}$$
 (5.13)

These equations can be used to determine the best fit to a particular charge versus exposure curve, knowing the rate of decline of the saturation current and the exposure range of interest.

For example, consider a discharge current curve with an initial saturation current,  $I_0$ , of 300 pA for an exposure rate of 0.1 R s<sup>-1</sup> and a continuous decline in the saturation current with  $m_{sat} = -2.0 \text{ pA s}^{-1}$ . The charge vs. exposure curve is shown in Fig. 5.4(b). The calibration factor using the initial saturation current is 3 nC R<sup>-1</sup>. After 3 R of exposure, the amount of charge depleted, from equation 5.5, is 8.1 nC which would be attributed to an exposure of 2.7 R using the calibration factor estimated from the initial saturation current, an error of 300 mR. This error can be decreased to zero by shifting the slope of the fitted line. The necessary slope can be determined from equation 5.9, substituting  $X_0 = 3$  R and solving for k. In this case,  $k = 2.70 \text{ nC R}^{-1}$  (shown in Fig. 5.4(b) as the fitted line). This factor would introduce errors at lower exposures which can be estimated from equation 5.12, with the maximum error below 3 R of  $q_m = -0.11$  nC, corresponding to an underestimate in the exposure of 41 mR, occurring at an exposure  $X_m$  of 1.5 R, from equation 5.11. The same error would occur at an exposure  $X_{m2}$  of 3.62 R, as seen in Fig. 5.4(b). Alternatively, the ideal value of k can be determined for a desired maximum error. For an error of no more than 0.03 nC or approximately 10 mR, the ideal calibration factor can be calculated by solving equation 5.12 to get  $k = 2.89 \text{ nC R}^{-1}$  with the maximum exposure at which this error occurs given by equation 5.13 and equal to 1.33 R.

### 5.3 VARIATION OF THE COLLECTOR RADIUS

# 5.3.1 The Collector Study

Ĭ

1

A personnel dosimeter must be capable of measuring exposures in the low mR range since a large proportion of all personnel exposures are in this range. It has been shown that the effect of increasing the air—gap is to increase the sensitivity however the strict linearity between charge density and exposure is lost with these

larger air—gaps. Another parameter that can be varied is the radius of the collector. This increases the collecting electrode's surface area thus increasing the sensitive volume.

A study was performed in which the radius of the collecting electrode was varied while the total radius of the collecting electrode and guard-ring stayed fixed at 24 mm. The radius of the polarizing electrode was also constant at 19 mm. A set of charge/discharge curves were acquired for four different collector radii -5, 10, 15, and 19 mm - for four different air-gaps -2, 4, 6, and 8.5 mm - at a range of voltages for a total of 59 configurations.

A set of discharge curves for a fixed air—gap ( $a=8.5\,\mathrm{mm}$ ) and a fixed charging voltage ( $V_o=170\,\mathrm{V}$ ) and the range of collector radii tested are shown in Fig. 5.5(a). The saturation current increased with increasing c due to the larger sensitive volume. For  $c=5\,\mathrm{mm}$ , the saturation current was relatively constant. However, at larger c, the saturation current was not constant but exhibited a continuous decline, just as observed in the guard—ring study for small guard—ring widths and larger air—gaps. Once again, the reason for this phenomenon is that with larger collector radii, ions are being collected from the fringe—field region at the edge of the electrodes. With the steady change in size of this region as the surface charge density varies, the saturation current does not have a constant value but continues to fall throughout the discharge process.

Another phenomenon becomes evident upon examination of the set of discharge curves for various collector radii with a=6.0 mm and  $V_0=400$  V (Fig. 5.5(b)). For  $c \le 15$  mm, the saturation current *increases* throughout the discharge process and peaks just before the final drop to zero. A possible explanation of this curious occurrence will be given in section 5.4.

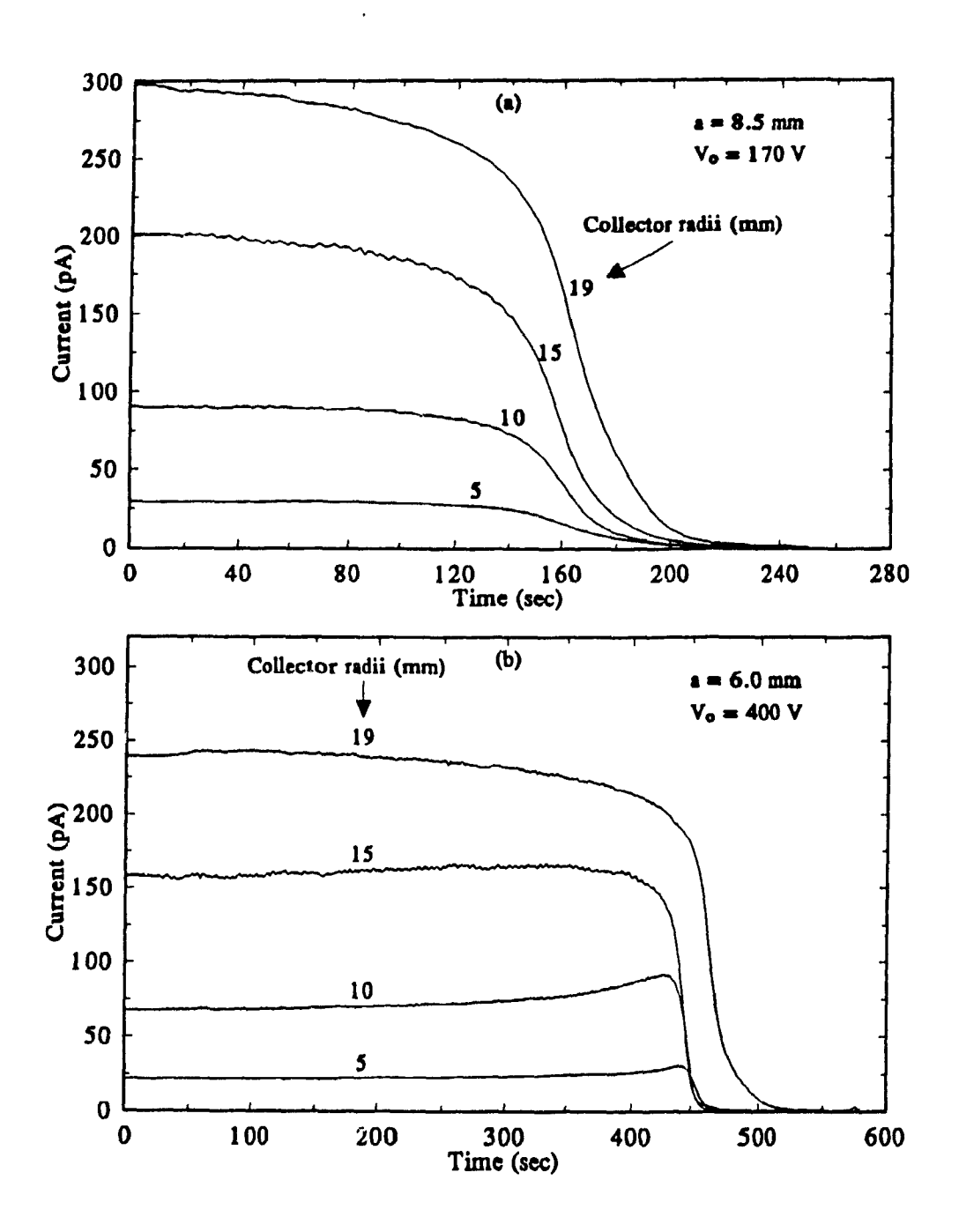


Figure 5.5 A set of discharge curves of current versus time (110  $\mu$ m Mylar electret) for dosimeters with (a) varying collector radii and constant air—gap and charging voltage and (b) different air—gap and charging voltage at 0.11 R s<sup>-1</sup>.

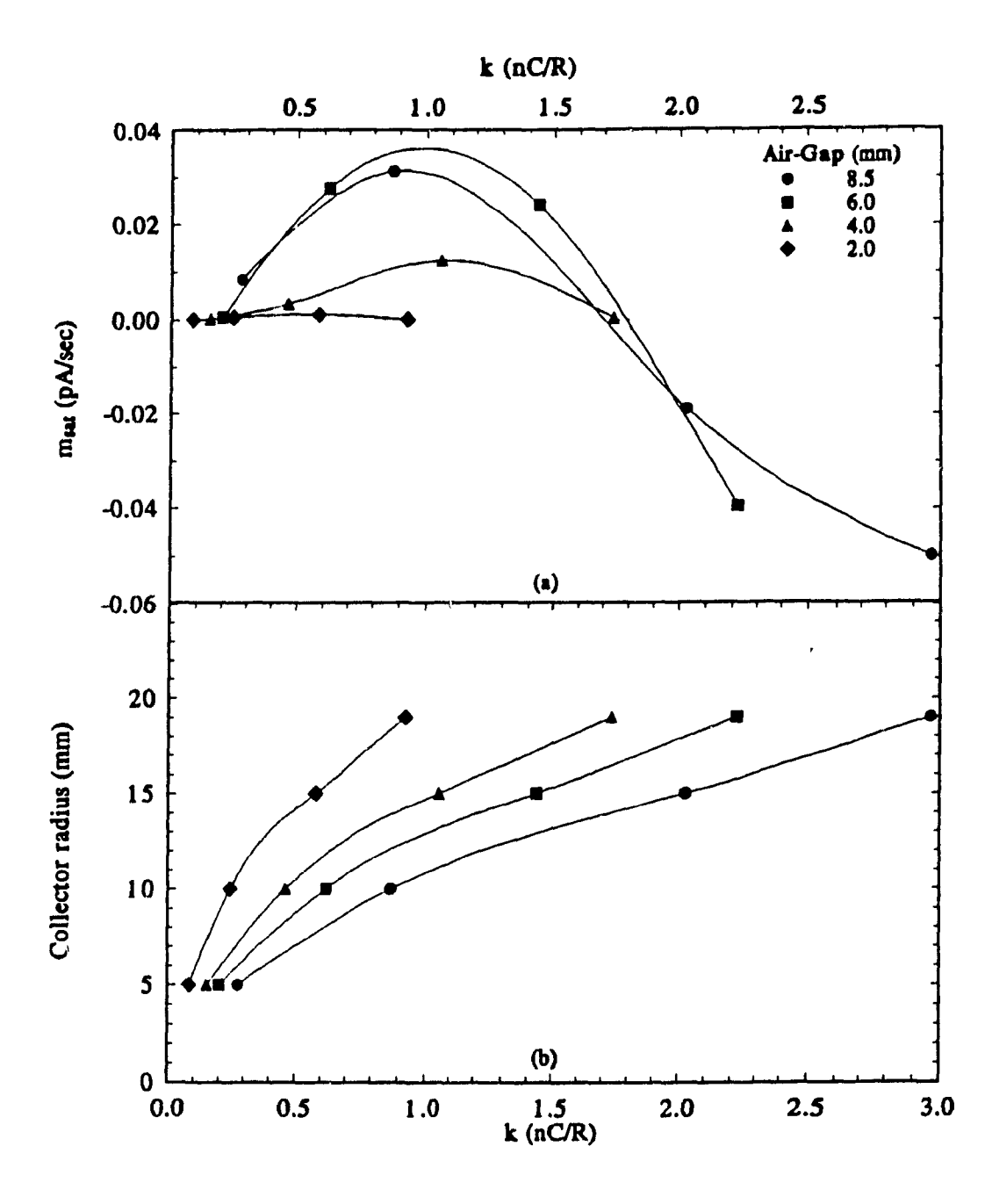
## 5.3.2 The Ideal Dosimeter Configuration

In order to simplify the use and understanding of the electret dosimeter, a dosimeter configuration in which the sensitivity is maximized while the linearity is retained must be determined. Sensitivity can be increased by increasing the air—gap, and by increasing the collector radius. The effect of the increase of each these parameters on the linearity—i.e. the value of  $m_{sat}$ —is different. In order to determine the ideal configuration, a plot of  $m_{sat}$  vs. k will yield the largest value of k for  $m_{sat}=0$  and the corresponding plot of c vs. k will indicate the collector radius for each particular air—gap and calibration factor. From Fig. 5.6 it is evident that the solution is not unique, however the geometry with a=4 mm and c=19 mm (from the lower plot) is a good compromise between a and c which maximizes k while keeping  $m_{sat}=0$ .

#### 5.4 SPATIAL CHARGE DENSITY INFORMATION

A table of  $\sigma_{max}$  for different collector radii (Table 5.1) reveals the fact that the average surface charge density decreases with increasing collector radius. The surface charge density should be constant across the surface of the electret for a fixed charge—up voltage. This measuring method is limited in that it gives the average signal over the whole collecting electrode area. It seems that the surface charge density is lower at the edge of the electret than at the middle. This would account for the measured surface charge density decreasing with increasing collector radius for a fixed voltage due to the inclusion of a larger portion of the fringe—field region.

Consider a dosimeter with a collecting electrode of radius u. This dosimeter is then charged to a voltage  $V_o$ . The final measured surface charge density  $\sigma_u$  is the average surface charge density over the whole collector of area  $A_u$ . Some



į

, r

Figure 5.6 (a) Slope of the initial flat portion of the current profile versus calibration factor for a range of different air—gaps and collector radii; (b) the corresponding plot of collector radius versus calibration factor for the same configurations.

Dosimeter Configuration		Charge Density (nC/cm <sup>2</sup> )		
$a \text{ (mm)} \qquad V_{o} \text{ (V)}$	c (mm)			
v	19	15	10	
170	3.84	3.93	4.21	
170	3.96	4.03	4.28	
80	1.90	1.95	2.03	
80	1.91	1.93	2.00	
	170 170 80	170 3.84 170 3.96 80 1.90	V <sub>o</sub> (V)     c (mm)       19     15       170     3.84     3.93       170     3.96     4.03       80     1.90     1.95	

Table 5.1 The total charge removed per unit area collector for different dosimeter configurations — for different air—gaps a and voltages  $V_o$  at different collector radii c — showing the increased charge density for smaller collector radii (110  $\mu$ m Mylar electret).

regions of the electrode may have a different charge density than others — i.e. the surface charge density may not be uniform across the whole electret — however it is the average charge density which is being detected. Consider another dosimeter with a collecting electrode of radius v, with v < u, charged to the same voltage,  $V_o$ . The average surface charge density over the electret area out to a radius u is the same as measured previously. The only difference is that the measured signal arises from a smaller area of the electret such that the final measured surface charge density  $\sigma_v$  is now the average charge density over the entire collector of area  $A_v$ . Multiplying each surface charge density by the area over which it applies and subtracting these two values results in the total surface charge  $q_{u-v}$  on a ring of the electret with an outer radius of v and inner radius of v,

$$\sigma_u A_u - \sigma_v A_v = q_{u-v} \tag{5.14}$$

Dividing this number by the area of the ring  $A_{u-v}$  gives the average surface charge density over the ring,

$$q_{u-v}/A_{u-v} = \sigma_{u-v} \tag{5.15}$$

The same process could then be applied to collecting electrodes with radii of v and w, u < v < w, resulting in the average surface charge density in a ring of outer radius w and inner radius v. Of course each ring could be made as narrow as physically possible resulting in a very large number of rings with a high degree of spatial resolution.

It is possible to take this method one step further. Information as to the charge state of the collecting electrode is known as a continuous function of time

through the discharge curve. By performing subtractions of the discharge curves themselves, the surface charge density of the whole electret surface can be determined as a continuous function of time or exposure.

\*

$$\sigma_{u-v}(t) = \frac{\sigma_u(t)A_u - \sigma_v(t)A_v}{A_{u-v}}$$
 (5.16)

The spatial resolution of the resulting surface charge density profile curve is limited by the number and size of the rings that were used to create it. The temporal resolution is limited only by the sampling rate of the signal – more than three points per second for the electrometer used.

Using this analysis, a plot of the surface charge density across the collector as a function of time for the discharge of a dosimeter with an air—gap of 6 mm and an initial charge—up voltage of 400 V is shown in Fig. 5.7(a). This curve was derived from the data in Fig. 5.5(b) where the annular rings are in increments of 5 mm, hence the spatial resolution is about 5 mm. The temporal resolution is approximately 0.3 seconds and is determined by the rate at which data points are collected from the electrometer. The center of the collector is located at 0 on the collector profile axis with the edges at +19 mm and at -19 mm.

The collector profile can be split up into three regions with Region I corresponding to the central portion of the collector, Region II being the area between the center of the collector and the edge, and Region III corresponding to the very edge of the collector. At the start of the discharge, the surface charge density was not uniform across the face of the collector but was lower at the edges of the collector as compared to the central portion. As the discharge progressed, Region I extending from about +10 mm to -10 mm, discharged at a fairly constant rate. Region III, the edges of the collector, discharged at a slower rate than the

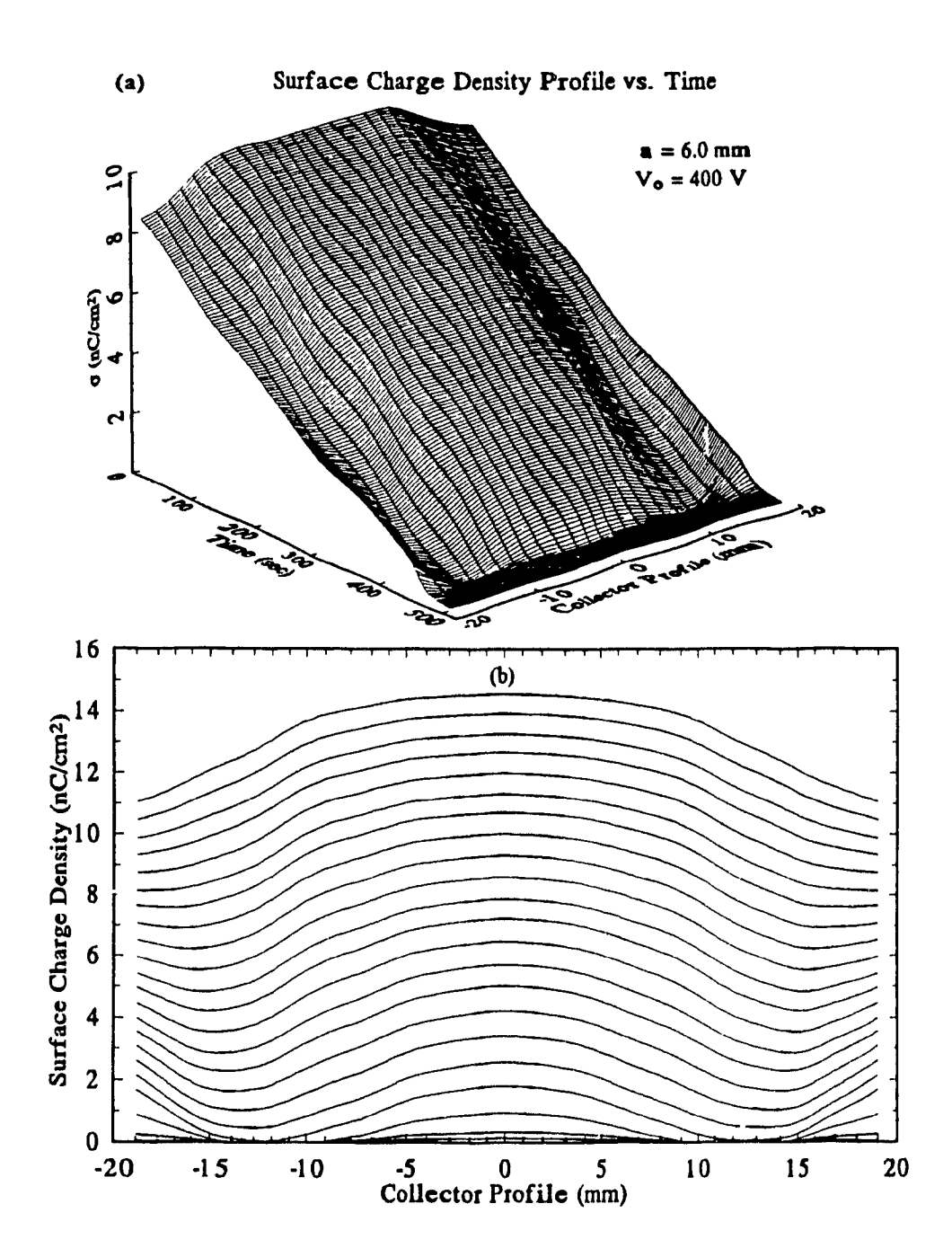


Figure 5.7 (a) Surface charge density of a 110  $\mu$ m Mylar electret across the collector as a function of time during the discharge process; (b) the same data plotted at every 25 second interval.

central portion. Region II, an area just inside the edge of the collector, extending from about 18 mm to 10 mm, discharged at a faster rate than both the edge and the center of the collector. This region moved in towards the center of the collector as the discharge continued as can be seen more clearly in a two dimensional plot of the same data, surface charge density vs. collector profile, at 25 second intervals (Fig. 5.7(b)). Initially, Region II extended from about 18 mm to 10 mm. Closer to the end of the discharge, this region extends from 15 to 5 mm. Once any portion of Region II reaches zero surface charge density, Regions I and and III quickly decayed to zero surface charge density as well.

No.

Ą

With this knowledge of the progression of the change in surface charge density, both spatially and temporally, across the collector in the discharge mode, the reasons for the different discharge current curves which exhibited decreases and increases ( $m_{sat}$  both positive and negative) in the saturation current can now be explained.

The steady decline in the saturation current is due to the fact that the collector radius is large enough to include all three regions, with the effect of Region III, with its rate of discharge being slower than the rest of the collector, being most dominant.

An increase in the saturation current will be observed if the collector radius initially only contains Region I, with its constant rate of decay, but as the discharge continues, contains an increasing portion of Region II, with its faster rate of decay, due to the fact that the inner radius of Region II is continually decreasing as the discharge progresses.

The saturation current remains constant if the collector radius is small enough and the guard—ring large enough such that no signal is measured from Regions II or III, or when the effect of these two regions cancels each other.

For example, if the collector radius for an air—gap of 6 mm was 10 mm, by examining Fig. 5.7(b) it is seen that initially it only contains Region I. Part way through the discharge process, the inner radius of Region II is seen to cross the 10 mm collector radius thus leading to a gradual increase in the measured current. Near the end of the discharge, Region I has almost disappeared with the inner radius of Region II being close to zero. At this point the current increases at a faster rate and subsequently plummets to zero once the charge layer has been fully depleted. The measured data confirms this explanation (see Fig. 5.5(b) for the 10 mm collector radius).

With a 19 mm collector radius, all three regions are included such that the net effect is the continual decrease in the saturation current due to the fact that the decrease in the rate of discharge in Region III is greater than the increase in the rate of discharge in Region II. This is again confirmed by the measured data (see Fig. 5.5(b) for the 19 mm collector radius).

It was observed that at the start of the discharge process, the surface charge density across the collector was not uniform but was at a slightly lower level at the edges of the collector. It could be argued that the variations in rates of discharge across the collector are solely due to this initial state. An experiment was performed to determine the effect of a uniformly charged collector on the discharge curve as compared to the discharge curves with an initially non-uniform charge distribution. A dosimeter with an 8 mm air—gap was charged to 170 V and then discharged. The discharge curve (shown in Fig. 5.8) exhibits the characteristic decline in the saturation current as the discharge progresses. The air—gap was decreased to 2 mm, and the dosimeter was again charged to 170 V. With this smaller air—gap, the final charge distribution is much more uniform than with the larger air—gap due to the much smaller size of the fringe—field at the edge of the

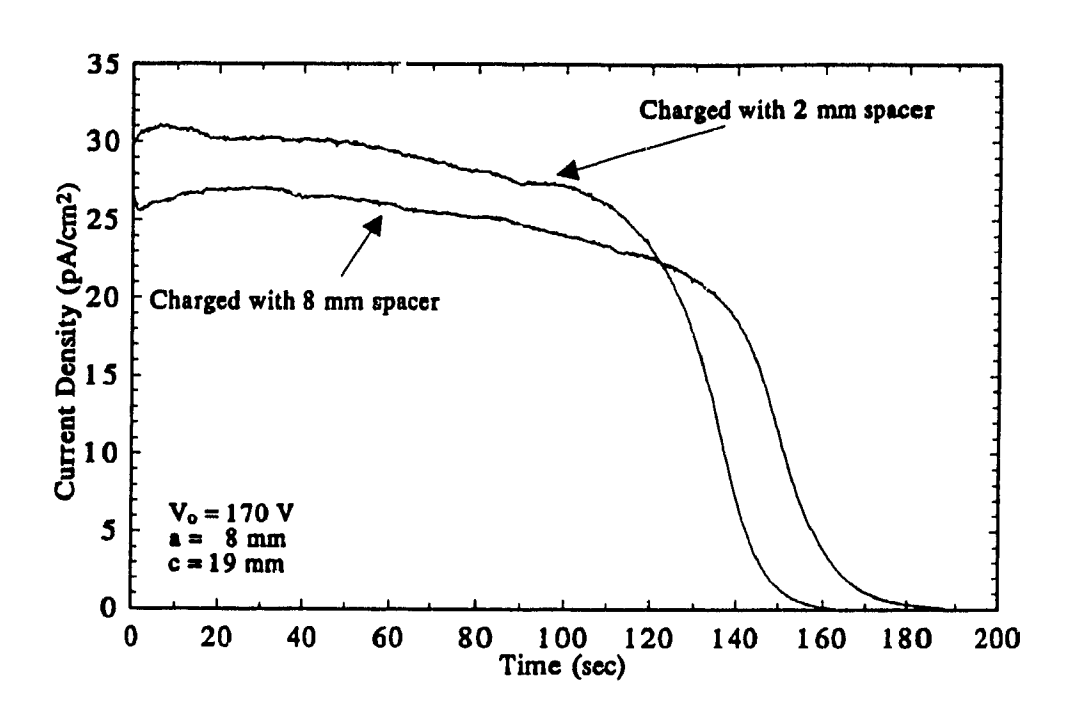


Figure 5.8 Two discharge curves of current density versus time for the same dosimeter charged with different air-gaps but discharged with the same air-gap (110  $\mu$ m Mylar electret, 0.11 R s<sup>-1</sup>).

electrodes. The air—gap was then increased back up to 8 mm and the dosimeter was discharged (Fig. 5.8). The resulting discharge curve exhibits the same decline in the saturation current. Therefore, the reason for the declining saturation current cannot be attributed to an initially non—uniform charge distribution. Further studies are required to provide an explanation of the shift in saturation current for dosimeters charged with different air—gaps but discharged with the same air—gap.

The proposed electret dosimeter has two opposing electrodes with a bakelite spacer ring keeping the two separated. The bakelite spacer-ring, an insulator, thus comprises the inside side-wall of the dosimeter. Some other electret dosimeters<sup>2,3</sup> are designed such that the side walls of the dosimeter are conductive and grounded during discharge, in addition to the grounding of the opposite electrode. The discharge curves for configurations with grounded walls were tested and found to exhibit the characteristic decline in the saturation current density with increasing exposure as was seen with the proposed electret dosimeter.

Knowledge of the spatial distribution of the surface charge density as a function of exposure is important for it explains many of the anomalous discharge curves that result with different dosimeter configurations. However, the overriding aim is to have a dosimeter with a measuring signal that is linear with exposure. It could be that a decreasing  $\jmath_{sat}$  due to the effect of Region III is compensated for by an increasing  $\jmath_{sat}$  due to the effect of Region II. The important fact is that the average saturation current density measured over the whole collector remains constant.

# REFERENCES

- U. W. Boag, "Distortion of the Electric Field in an Ionization Chamber due to a Difference in Potential between Guard Ring and Collector", Phys. Med. Biol., 9, 25-32, 1964.
- <sup>2</sup>G. Pretzsch, et al, "Measurement of Tritium Activity Concentration in Air by Means of the Electret Ionisation Chamber", Rad. Prot. Dos. 12, 345-349, (1986).
- <sup>3</sup>G. Pretzsch, B. Dörschel, "A Re-usable Electret Dosimeter", Rad. Prot. Dos. 12, 351-354, (1986).

### CHAPTER 6

### **ENERGY DEPENDENCE**

### 6.1 INTRODUCTION

An important quality of any dosimeter is the dosimeter's dependence on the energy of the incoming radiation. Ideally the dosimeter's response would be independent of the photon energy and would be solely dependent on the radiation exposure. Practically this never occurs. Instead the energy dependence must be minimized by the proper choice of materials used in the construction of the dosimeter.

There are basically three reasons for the possible energy dependence of the proposed electret dosimeter. At low energies, primary photons are attenuated in the wall of the dosimeter. A peak in the photoemission current from the polarizing electrode could result in an over—response at intermediate energies. The possible loss of electronic equilibrium conditions would result in a decreased response at high energies.

### 6.2 LOW ENERGIES

The attenuation of low energy photons in the wall of the dosimeter is inevitable with any thickness of wall material. The only possible way of circumventing this problem is to not have a wall as with the standard free—air ion chamber. This is not practical for a personnel dosimeter. The half—value layer of photons in the very low energy range of 2 to 10 keV ranges from 11  $\mu$ m to 1.3 mm in water and 1.1  $\mu$ m to 100  $\mu$ m in aluminum; therefore even the very thinnest of wall materials will attenuate these low energy photons. In order to minimize this, the density, effective atomic number, and thickness of the electrode wall material can be minimized.

The effect of the attenuation of low energy photon beams by the wall of the dosimeter was studied. Fig 6.1(a) shows an energy response curve for two different dosimeter wall materials – 0.8 mm thick bakelite and 1.5 mm thick fiberglass. The dosimeter signal has been normalized to the value at 29 keV. The reduced response at lower effective photon energies is apparent with the reduction greater for the thicker wall – down to 91 % at 19 keV for the bakelite and 62 % at 19 keV for the fiberglass wall.

#### 6.3 INTERMEDIATE ENERGIES

The energy dependence of the electret dosimeter was measured at intermediate energies using a Philips orthovoltage radiotherapy unit with effective energies ranging from 51 to 128 keV. An over-response of the dosimeter was registered for energies below 100 keV. The factor by which the response was increased at lower energies was found to be dependent on the air-gap as seen in Fig. 6.1(b) which plots the energy dependence for air-gaps of 2, 4, and 6 mm for a 19 mm collecting electrode. For smaller air-gaps, a larger proportion of the total signal is due to photoemission from the polarizing electrode hence the dependence on energy will be much more pronounced at smaller air-gaps, whose proportion of photoemission current to total signal is large, than at large air-gaps, whose proportion of photoemission to total signal is smaller.

The existence of this peak at intermediate energies depends on the effective atomic number  $Z_g$  of the material of or surrounding the sensitive volume. Fig. 6.2(a), adapted from Attix<sup>1</sup>, illustrates schematically three typical energy dependence curves for a dosimeter with a sensitive volume consisting of a material with atomic number greater than, equal to, or less than the effective atomic number of air. At low energies all three curves exhibit a decrease in relative response to  $^{60}$ Co gamma rays due to the attenuation of low energy photons in the wall of the

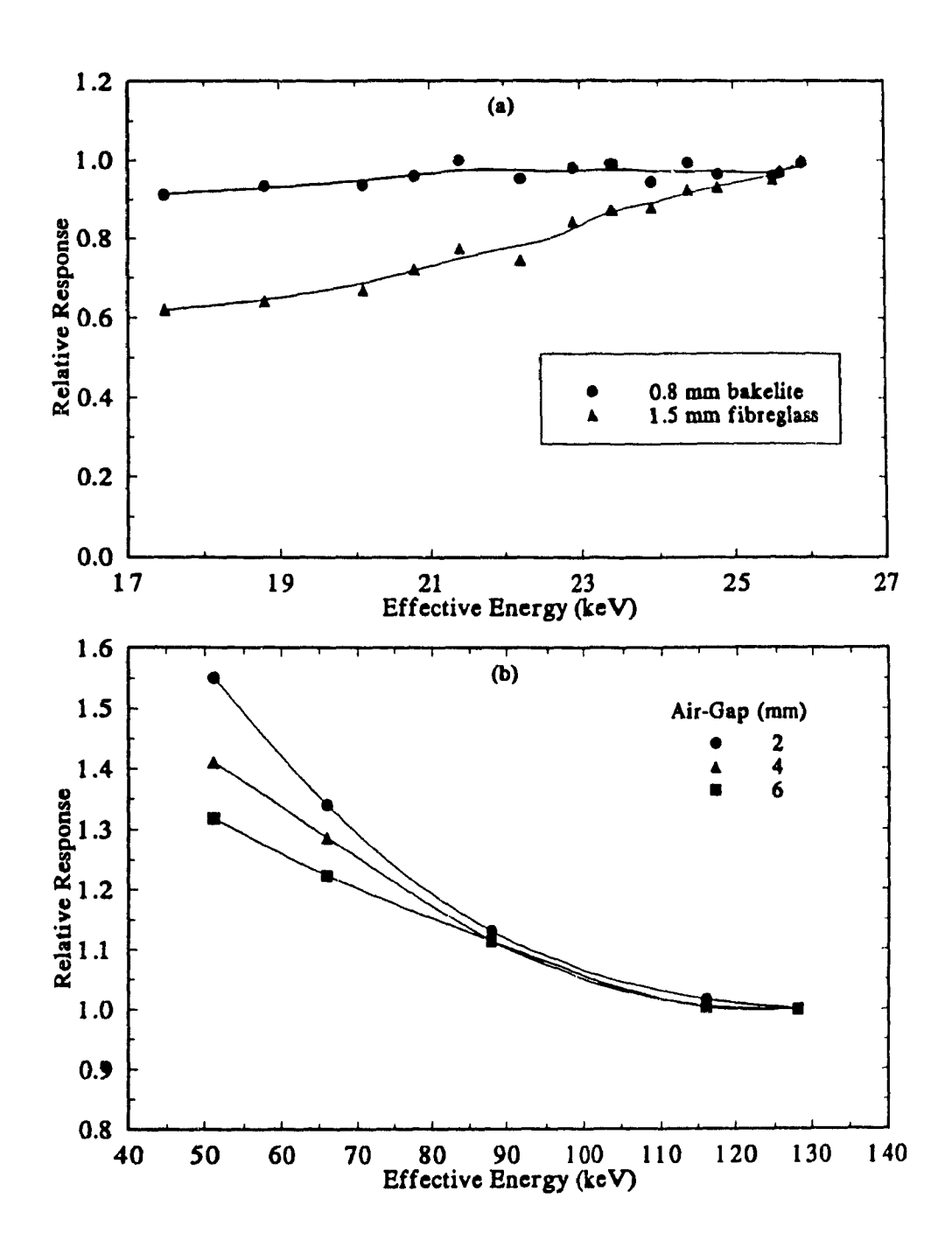


Figure 6.1 (a) Relative response of the dosimeter to low energy x-rays for two different dosimeter electrode-backings, a = 3 mm; (b) relative response at intermediate energies for different air-gaps.

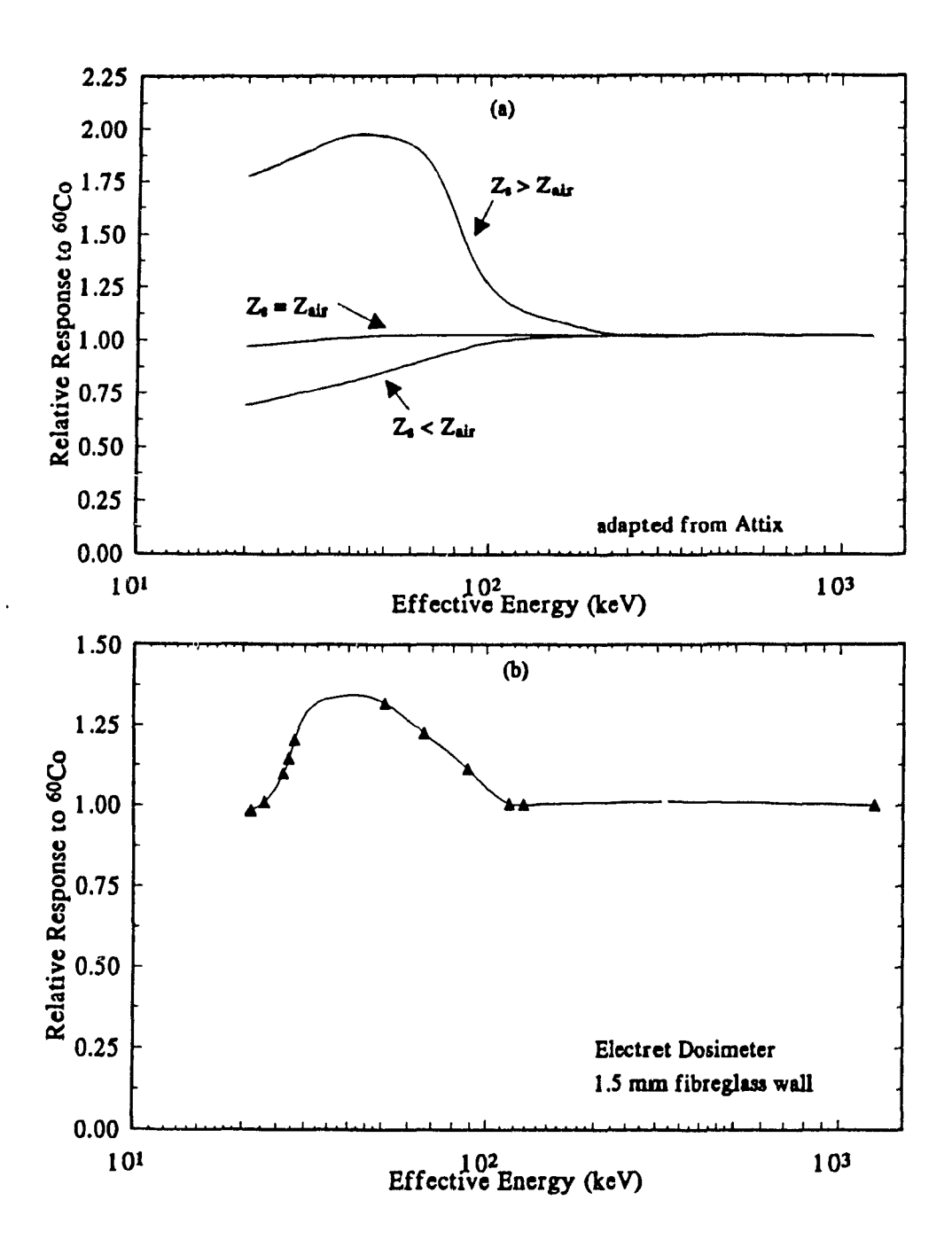


Figure 6.2 (a) A schematic plot (adapted from Attix<sup>1</sup>) showing the effect of the atomic number of or surrounding the sensitive volume  $Z_s$  as compared to that of air on a dosimeter's energy dependence; (b) the overall energy dependence for the electret dosimeter for a=6 mm with a 110  $\mu$ m Mylar electret.

dosimeter. For  $Z_s > Z_{air}$  an over-response of the dosimeter to photons of energies between 30 and 100 keV is evident. This is a result of the photoelectric effect being proportional to  $Z^{3.8}$  and to  $(h\nu)^{-3}$  (see section 44). To reduce this energy dependence,  $Z_s$  can be made equal to  $Z_{air}$ , as shown in the diagram. For the electret dosimeter, although the sensitive volume consists of air, the material surrounding the sensitive volume is not. The boundaries of the sensitive volume are the polarizing electrode, the dielectric material covering the collecting electrode, and the side-wall of the spacer-ring used to provide a fixed electrode spacing. To minimize the effect of these materials on the energy dependence of the dosimeter, the effective atomic number of each should be close to that of air. By replacing the aluminum polarizing electrode (Z = 13) with a graphite electrode (Z = 6), this over-response will be much reduced resulting in a dosimeter with almost no energy dependence (as measured with an electret dosimeter designed by Gupta et al.2).

# 6.4 HIGH ENERGIES

At high energies, problems involving the loss of electronic equilibrium conditions may become important. This again involves the thickness of the wall of the dosimeter except now the wall must be made thick enough to result in electronic equilibrium conditions holding for a particular photon energy  $-0.5 \text{ g/cm}^2$  for  $^{60}\text{Co}$  gamma rays<sup>3</sup>.

The electret dosimeter with a 1.5 mm fiberglass wall (along with the 110  $\mu$ m Mylar electret with its aluminized backing) exhibited a saturation current at Cobalt-60 energies – for a 2 mm air-gap – that was within 0.7 % of the value expected from measurements with a calibrated ion chamber (see section 44), hence this wall came close to being sufficiently thick to produce electronic equilibrium at this energy. The thinner walled chambers which perform better at low energies,

with less attenuation of the low energy photons, have insufficient wall material for the h gher energies (the 0.75 mm fiberglass walled chamber with a 25  $\mu$ m aluminized Teflon electret has a saturation current for the same air—gap 17 % below the expected value).

10000

## 6.5 OVERALL ENERGY DEPENDENCE

1

The energy dependence curve for the electret dosimeter with a 1.5 mm fiberglass wall and a 6 mm air—gap is shown in Fig. 6.2(b). All the above—mentioned effects are evident: the attenuation at very low photon energies, the over—response of the dosimeter to photons in the energy range 30 to 100 keV due to the photoemission current, and the maintenance of electronic equilibrium for this wall thickness at Cobalt energies. The general shape of this curve, with the peak at lower energies and the energy independence at higher energies, is in agreement with that of an electret dosimeter constructed by Dorschel and Pretzsch<sup>4</sup>, except their dosimeter exhibited a higher peak at low energies.

For comparison purposes, the energy dependence curves for a LiF TLD and a typical film badge dosimeter are shown in Fig. 6.3.

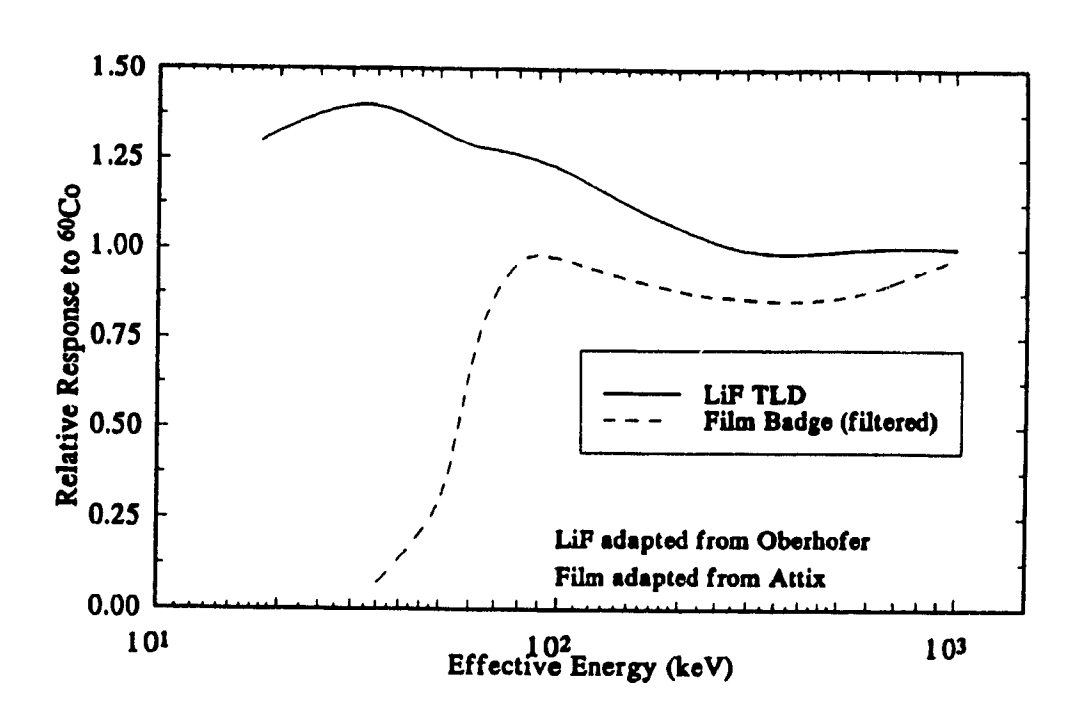


Figure 6.3 Typical energy dependence curves for a LiF TLD and a filtered film badge (adapted from Oberhofer<sup>5</sup> and Attix<sup>6</sup> respectively).

## REFERENCES

- <sup>1</sup>F. H. Attix, Introduction to Radiological Physics and Radiation Dosimetry, (John Wiley and Sons, New York, 1986), p.285.
- <sup>2</sup>P. C. Gupta, P. Kotrappa, and S. K. Dua, "Electret Personnel Dosemeter", Rad. Prot. Dos. 11, 107-112 (1985).
- <sup>3</sup>H. E. Johns, J. R. Cunningham, *The Physics of Radiology*, (Charles C Thomas, Springfield, Illinois, 1983), p.240.
- <sup>4</sup>B. Dörschel, G. Pretzsch, "Properties of an Electret Ionisation Chamber for Individual Dosimetry in Photon Radiation Fields", Rad. Prot. Dos. 12, 339-343 (1986).
- <sup>5</sup>G. Portal, M. Oberhofer and A. Scharmann (Eds.), Applied Thermoluminescence Dosimetry, (Adam Hilger Ltd, Bristol, 1981), p.104.
- <sup>6</sup>F. H. Attix, Introduction to Radiological Physics and Radiation Dosimetry, (John Wiley and Sons, New York, 1986), p.415.

#### CHAPTER 7

#### CONCLUSION

## 7.1 SUMMARY

The electret dosimeter has not yet attained the level of commercialization currently held by thermoluminescent dosimeters, pocket ionization chambers, and film dosimeters. This work has detailed a possible improvement in the field of electret dosimetry with the use of a new charging technique and an alternative method of read—out. These modifications simplify the regular use of the electret dosimeter and bring the electret dosimeter one step closer to full scale use.

The isothermal charging technique used to charge the dosimeter was described. The need for saturation conditions to exist throughout the regular use of the dosimeter was detailed by analyzing the discharge process and defining the calibration factor. The effect of various parameters on the sensitivity and exposure range of the dosimeter was discussed. Exposure ranges from low mR to hundreds of R are possible with the appropriate dosimeter configuration. A comparison of this read—out technique with the voltage read—out method was presented. This led to a discussion of possible problems with the charging technique associated with radiation induced conductivity in the polymer and other problems encountered with virgin Teflon polymers.

The phenomenon of electrode edge effects was explained detailing the need for a minimum size guard-ring for a given air-gap. An analytic method by which to minimize the errors associated with this effect was presented. A method of determining the ideal dosimeter configuration that maximizes sensitivity while minimizing electrode edge effects was developed. This involved the determination of the spatial distribution of the electret's charge density as a continuous function of exposure. Analysis of the resulting plots of charge density versus exposure versus

position provided an explanation for the deviation of the charge/discharge curve from the ideal theory.

Finally, the energy dependence of the dosimeter was presented. This was shown to be due to: attenuation of low energy photons in the wall of the dosimeter; a possible over—response of the dosimeter at intermediate energies depending on the atomic number of or surrounding the sensitive volume; and the possible under—response at high energies due to a loss of electronic equilibrium conditions. Methods by which to minimize this dependence were also detailed.

For comparison with other personnel and electret dosimeters, the features of the proposed electret dosimeter are summarized below:

# Reusability:

The dosimeter is inherently reusable. After each use the dosimeter is simply recharged up to the desired voltage and used again. The effects of an earlier exposure are easily purged with no shift in sensitivity due to earlier exposures. The reusability of a dosimeter is important in that it allows individual calibration, whereas single—use dosimeters such as film badges must be batch—calibrated—either calibration mode can be used with the electret dosimeter.

#### Linearity:

The linear relationship between the charge removed from the electret and the exposure holds over the entire exposure range and simplifies the process of calibration.

# Exposure Range:

One dosimeter covers the entire exposure range normally encountered in personnel dosimetry, from low mR to hundreds of R, without the need for multiple sensing elements — one being for high exposures and the other for low.

# Exposure Rate:

The only low exposure—rate limitation is that due to uncertainties imposed by charge decay. At high exposure rates, not normally encountered in personnel dosimetry, recombination effects will become significant, just as with regular ionization chambers.

# Energy Dependence:

The dependence of response on photon energy can be made to be minimal since air is the measuring medium. Influences of the materials surrounding the sensitive volume can result in a large energy dependence; however, with the proper choice of materials, this effect can be minimized.

# Stability:

There is a slight fading of the signal which begins as soon as the dosimeter is initially charged. This can be accounted for in the determination of exposure.

## Temperature:

Variations within the normal temperature range encountered in everyday use have no effect on the dosimeter due to the fact that the signal, charge trapped on the polymer surface, is stable; however the effect of a continuous elevated temperature is similar to that of TLDs in that the signal will fade since the energy traps in which the charges are trapped are of finite depth.

## Humidity:

For a Tesson electret, the effect of increased levels of humidity is expected to be minimal due to the hydrophobic nature of Tesson.

#### Shock:

The dosimeter is inherently shock—resistant since the signal is not mechanical but relies on the trapping of charges in deep energy traps in the polymer.

#### Cost:

A personnel dosimeter intended for regular use by radiation workers, hospital workers, and industry workers must be inexpensive. The proposed electret dosimeter is very inexpensive since the only materials needed are fiberglass boards, or some other stiff material, a piece of aluminized Teflon, and graphite or aluminum foil.

#### Read-Out:

Read—out involves measuring the total charge released upon irradiation of the dosimeter. The exposure rate during the final discharge need not remain constant during the read—out or from read—out to read—out. The only components required for a complete electret dosimetry system are a calibrated electrometer and a radiation source.

## Design:

A dosimeter meant for large—scale use would not require screws but could simply be glued together since interchangeable spacer—rings would not be necessary. The electrical pin connections could be discarded and the exposed wire filed flush with the surface of the electrode backing material. An attachment on the incoming wire would provide a solid, electrical pressure—contact with the exposed wire of the dosimeter. The dosimeter would then be a smooth, lightweight cylinder, with no protruding parts, of radius 2.5 cm, and height 0.7 cm.

# Computer Automation:

A system could be designed whereby a dosimeter would enter an irradiator from a container holding a large number of dosimeters and slide into a holder where the electrical connections would be engaged. The dosimeter would then be irradiated. A computer monitoring the current would: stop the discharging process once the current reached zero; display the total charge

removed and the exposure knowing the initial charge on the dosimeter and the length of time the dosimeter has been in use (this information would be in memory), and the dosimeter's calibration factor (in memory and verified during the discharge process); apply the external potential and continue irradiation until the current reached zero once again; halt the irradiation; display the total charge deposited; eject the dosimeter; and repeat the whole process for subsequent dosimeters.

#### 7.2 FUTURE WORK

The full effect of radiation—induced conductivity (RIC) on the electret dosimeter must be further explored in two areas. The first area is obviously in the field of charge retention. One of the criticisms that can be leveled at this charging technique is that it involves the irradiation of the polymer and hence the effects of RIC which decreases charge stability are unavoidable. This charging technique could be simply modified by placing the dosimeter vertically under the radiation source and covering the side of the dosimeter that the polymer is on with lead thus avoiding the irradiation of the polymer but still irradiating a large portion of the sensitive volume necessary for charge carrier creation—feasible for chambers with a minimum size air—gap. The effect of this on charge retention should be studied. The second area involves effects of RIC during use in the field. It is not possible to shield the polymer from irradiation during regular use with any electret dosimeter. As seen in section 4.6.2, the currents due to RIC and DRIC are not negligible. These currents are proportional to the electric field in the polymer which changes as the surface charge on the polymer is depleted.

Further studies are required to explain the difference in saturation currents for dosimeters charged with different air—gaps but discharged with the same air—gap, as seen at the end of section 5.4. Work must also continue in the determination of the magnitude of the errors introduced in taking charge decay into account, as seen in section 4.6.4.

The possibility of using a modified electret dosimeter for neutron and electron dosimetry could also be studied.

# **BIBLIOGRAPHY**

- F. H. Attix, Introduction to Radiological Physics and Radiation Dosimetry, (John Wiley and Sons, New York, 1986).
- H. Bauser and W. Ronge, "The Electret Ionization Chamber: A Dosimeter for Long-Term Personnel Monitoring", Health Phys., 34, 97-102 (1978).
- J. W. Boag, "Distortion of the Electric Field in an Ionization Chamber due to a Difference in Potential between Guard Ring and Collector", Phys. Med. Biol., 9, 25-32, 1964.
- P. W. Chudleigh, R. E. Collins, and G. D. Hancock, "Stability of Liquid Charged Electrets", Appl. Phys. Lett., 23, 211-213, 1973.
- B. Dörschel and G. Pretzsch, "Properties of an Electret Ionisation Chamber for Individual Dosimetry in Photon Radiation Fields", Rad. Prot. Dos. 12, 339-343 (1986).
- G. W. Fabel and H. K. Henisch, "Polymer Thermoelectret Dosimetry", Phys. Status Solidi A 6, 535-541 (1971).
- B. G. Fallone and E. B. Podgorsak, "Production of Foil Electrets by Ionizing Radiation in Air", Phys. Rev. B 27, 2615-2618 (1983).
- B. G. Fallone and E. B. Podgorsak, "Dynamics of radiation-induced charging and discharging of foil electrets", Phys. Rev. B 27, 5062-5065 (1983).

- B. G. Fallone and J. A. Bencomo, "A linear—quadratic fit for saturation curves obtained under continuous irradiation of parallel—plate ionization chambers", Med. Phys. 14, 359—364 (1987).
- B. G. Fallone and E. B. Podgorsak, "Saturation curves of parallel-plate ionization chambers", Med. Phys. 10, 191-196 (1983).
- B. G. Fallone and E. B. Podgorsak, "Radiation-induced foil electret chamber", Phys. Rev. B 28, 4753-4760 (1983).
- P. C. Gupta, P. Kotrappa, and S. K. Dua, "Electret Personnel Dosemeter", Rad. Prot. Dos. 11, 107-112 (1985).
- O. Heaviside, "Electromagnetic Induction and its propagation. Electrization and Electrification. Natural Electrets", The Electrician, 230-231, 1885.
- G. Hine and G. Brownell, Radiation Dosimetry, (Academic Press Inc., New York, 1956).
- M. Ikeya, K. Mahesh and D. R. Vij (Eds.), Techniques of Radiation Dosimetry, (John Wiley & Sons, New York, 1985).
- H. E. Johns and J. R. Cunningham, *The Physics of Radiology*, (Charles C Thomas, Springfield, Illinois, 1983).
- B. MacDonald, "Surface Charge Characteristics of the Radiocharged Electret", M.Sc. thesis, McGill University, 1990.

- H. B. Marvin, "How to measure radiation with electrets (U.S. Patent No. 2,695,363)", Nucleonics 13, 82-83 (1955)
- G. Mie, "Der Elektrische Strom in Ionisierter Luft in Einem Ebenem Kondensator", Ann. Phys. 13, 857-889 (1904).
- M. Oberhofer and A. Scharmann (Eds.), Applied Thermoluminescence Dosimetry, (Adam Hilger Ltd, Bristol, 1981).
- M. M. Perlman and S. Unger, "Electron bombardment of electret foils", Appl. Phys. Lett. 24, 579-580 (1974).
- G. Pretzsch, B. Dörschel, and B. Leuschner, "Investigation of Teslon Electret Detectors for Gamma Dosimetry", Rad. Prot. Dos. 4, 79-84 (1983).
- G. Pretzsch, et al, "Measurement of Tritium Activity Concentration in Air by Means of the Electret Ionisation Chamber", Rad. Prot. Dos. 12, 345-349, (1986).
- G. Pretzsch, B. Dörschel, "A Re-usable Electret Dosimeter", Rad. Prot. Dos. 12, 351-354, (1986).
- D. A. Seanor (Ed.), Electrical Properties of Polymers, (Academic Press, New York, 1982).
- H. Seeman, "Messung der Sättigungsstromkurve in Luft, die mit Röntgenstrahlen ionisiert ist", Ann. Phys. 38, 781-785 (1912).

- G. M. Sessler (Ed.), Topics in Applied Physics Vol.33: Electrets, 2nd ed. (Springer-Verlag, New York, 1987).
- G. M. Sessler, "Electric Fields and Forces due to Charged Dielectrics", J. Appl. Phys., 43, 405-408, (1972).

1